UCRL 10342

University of California

Ernest O. Lawrence Radiation Laboratory

TWO-WEEK LOAN COPY

This is a Library Circulating Copy which may be borrowed for two weeks. For a personal retention copy, call Tech. Info. Division, Ext. 5545

MASS-ENERGY RELATIONS IN THE FISSION OF HIGHLY EXCITED HEAVY NUCLEI

Berkeley, California

DISCLAIMER

This document was prepared as an account of work sponsored by the United States Government. While this document is believed to contain correct information, neither the United States Government nor any agency thereof, nor the Regents of the University of California, nor any of their employees, makes any warranty, express or implied, or assumes any legal responsibility for the accuracy, completeness, or usefulness of any information, apparatus, product, or process disclosed, or represents that its use would not infringe privately owned rights. Reference herein to any specific commercial product, process, or service by its trade name, trademark, manufacturer, or otherwise, does not necessarily constitute or imply its endorsement, recommendation, or favoring by the United States Government or any agency thereof, or the Regents of the University of California. The views and opinions of authors expressed herein do not necessarily state or reflect those of the United States Government or any agency thereof or the Regents of the University of California.

Research and Development

UCRL-10342
UC-34 Physics
TID-4500 (17th Ed.)

UNIVERSITY OF CALIFORNIA

Lawrence Radiation Laboratory
Berkeley, California

Contract No. W-7405-eng-48

MASS-ENERGY RELATIONS IN THE FISSION OF HIGHLY EXCITED HEAVY NUCLEI.

Eldon Lee Haines

(Ph.D. Thesis)

June 29, 1962

Printed in USA. Price $2.00. Available from the
Office of Technical Services
U. S. Department of Commerce
Washington 25, D.C.

MASS-ENERGY RELATIONS IN THE FISSION OF HIGHLY EXCITED HEAVY NUCLEI

Contents

	Abstract	v
I.	Introduction	1
II.	Experimental	
	A. Equipment	3
	B. Bombardment Procedures	5
III.	Calculations	9
	A. Calculation of Laboratory Energies	9
	B. Transformations	11
	C. Moments in the Description of the Contour Maps	12
	D. Errors in the Mean and Variance of the Distributions	17
IV.	Results	21
V.	Discussion	
	A. Kinetic-Energy Distributions	31
	B. Mass Distributions	33
	C. Remarks Concerning the Excitation Energy	38
VI.	Appendices	
	A. Some Experimental Details	41
	B. Data Processing	45
	C. Corrections	54
	Acknowledgments	76
	References	77

MASS-ENERGY RELATIONS IN THE FISSION OF HIGHLY EXCITED HEAVY NUCLEI

Eldon Lee Haines

Lawrence Radiation Laboratory
University of California
Berkeley, California

June 29, 1962

ABSTRACT

Mass-energy relations in the fission of the compound nucleus Fm^{254} have been studied at excitation energies in the range from 58 to 116 MeV. This compound nucleus was produced by bombardments of Th^{232}, U^{238}, and Pu^{242} with the heavy ions Ne^{22}, O^{16}, and C^{12}, respectively. The kinetic energies of the two fission fragments from each event were measured using semiconductor detectors. From these energies the masses and total kinetic energies were calculated.

The kinetic-energy distributions as a function of mass asymmetry, and the mass distributions as a function of the kinetic energy were studied. It was found that the average kinetic energies were consistent with those expected from electrostatic repulsion of the two fragments at a nearly constant separation. The bell-shaped mass distributions narrowed rapidly as the kinetic energies of the fragments increased. The quantitative behavior of this narrowing suggests that most of the initial excitation energy of the compound nucleus is not available either for conversion into kinetic energy of the fragments or for the production of asymmetric mass divisions that are energetically unfavorable.

I. INTRODUCTION

When elements heavier than radium are bombarded with charged particles, the most probable reaction is binary fission. The probability that a compound nucleus will de-excite to its ground state by particle emission is very small. If the projectiles are protons, deuterons, or α particles, direct interactions may compete actively with compound-nucleus formation. The resulting fission occurs at a wide variety of excitation energies, which makes interpretation of the data difficult and ambiguous.

It is well known that at low excitation energies these heavy elements fission asymmetrically. As the excitation energy is increased, symmetric fission begins to compete favorably with asymmetric fission.[1] Until recently, the study of mass distributions of fission products at high, well-defined excitation energies has not been possible.

The study of the kinetic energy released in the fission process has been similarly limited to nuclei of low initial excitation energy. The average kinetic energy of the fragments has long been seen to remain constant with small changes in excitation.[2,3] But changes in the kinetic-energy distributions could not be studied in detail over a large range of excitation energies.

Use of heavy-ion acclerators has made possible very high, well-defined excitation energies.[4] Although a 160-MeV O^{16} ion, for example, has the same velocity as a 40-MeV α particle, much greater excitation can be introduced in a reaction by the O^{16} ion without increasing the probability for direct interactions.

A study of mass-energy relations in the fission of highly excited heavy nuclei is reported here. The compound nucleus studied was Fm^{254}, with excitation energies ranging from 58 to 116 MeV. This compound nucleus was created in the following three ways:

a. $C^{12} + Pu^{242}$

b. $O^{16} + U^{238}$

c. $Ne^{22} + Th^{232}$.

The experiments involved measurement of the kinetic energies of the two fission fragments for each event. From conservation of linear momentum and conservation of mass, the masses of the fragments were determined. Variations in the distributions of the mass and total kinetic energy were studied by the method of moments.

II. EXPERIMENTAL

A. Equipment

1. Heavy Ion Beams

Heavy-ion beams with a constant velocity of $(10.3 \pm 0.1 \text{ MeV/nucleon})^{1/2}$ were supplied by the Berkeley heavy-ion linear accelerator (Hilac).[5] To reduce energies of the heavy ions to the desired values, aluminum foils of known thickness were placed in the beam path between two collimators. The foil thickness required for a given energy degradation was determined from Northcliffe's range-energy curves for heavy ions.[6]

2. Fission Chamber

The fission chamber, approximately 60 cm in diameter, has two detector arms whose angular positions can be adjusted from outside the chamber (Fig. 1). In addition, the radial position of each detector and the amount of absorber in the beam path can be controlled without opening the chamber. The target mount extends through the top of the chamber, making the target angle adjustable from outside. A permament magnet at the mouth of the Faraday cup prevents electrons from entering or leaving the cup. The vertical collimators, each 2 by 6 mm, are 60 cm apart. The second is only 5 cm from the target.

3. Electronic System

Gold surface-barrier detectors, similar to those described by Blankenship, were used for detection of the fragments and measurement of their energies.[7] For most of the measurements, 13/16-in.-diam. detectors made from 150-Ω-cm n-type silicon were used. These gave linear calibration curves when operated at reverse biases of 3 to 6 V. Judged by their response to the single-fragment energy spectrum of Cf^{252}, the detectors showed good energy resolution. However, they did display an aberration commonly called "pulse-height defect". This is discussed in Appendix C.5.

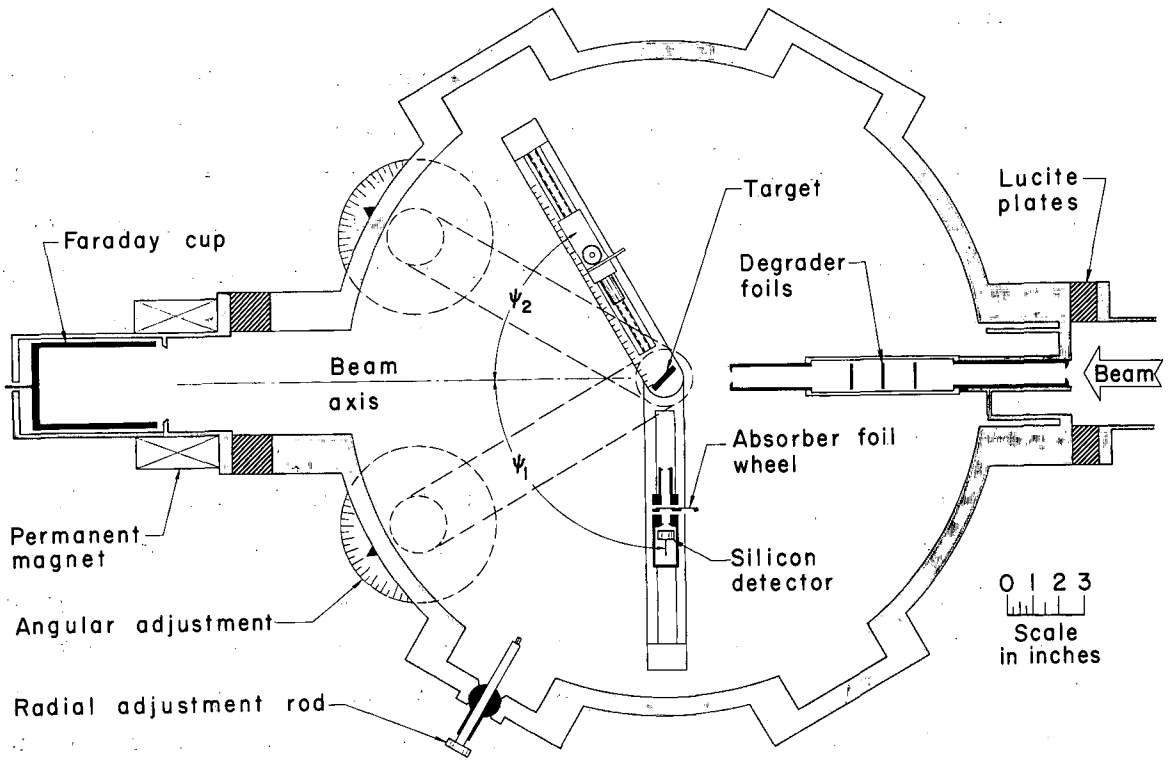

MUB-716

Fig. 1. Fission chamber. In the experiments described here, the detector located at angle ψ_2 was larger than that shown in the figure. Thus it could detect all fission fragments in coincidence with those striking the detector at the angle ψ_1.

The electronic system (Fig. 2) was composed of three interdependent parts. The linear systems amplified the pulses from each detector for pulse-height analysis. The coincidence system time-resolved the two pulses. Only pulses occurring within 10^{-8} sec of one another were accepted. Finally, a two-dimensional analyzer, activated by the coincidence system, measured the linear pulse heights and stored the results on magnetic tape. The details of this system are given in Appendix A.1.

4. Targets

The Pu^{242} and Th^{232} targets were prepared by electrodepositing the metal oxides onto thin nickel foils. A 250-$\mu g/cm^2$-thick Pu target was used in these experiments; the Th target thickness was 300 $\mu g/cm^2$. The U^{238} target, prepared by vaporization of UF_4, was 110 $\mu g/cm^2$ thick. The thickness of these targets was found by measuring the alpha decay rate on a known area. The Au^{197} target used for calibrating the linear systems was a 1/4-mil Au foil (see section B-1 below). Its thickness was determined by the extent to which it degraded the energies of fragments from the spontaneous fission of Cf^{252}. Preparation of these targets is discussed more fully in Appendix A.2.

B. Bombardment Procedures

1. Calibration of the Linear Systems and the Two-Dimensional Analyzer

Calibration of the linear systems depended on the fact that fragments from heavy-ion-induced fission have higher energies when observed at forward angles than at backward angles. The high momentum of the energetic heavy ion imparts a high velocity to the fissioning nucleus. This velocity becomes a component of each fragment's laboratory (lab) velocity, causing its lab energy to be dependent on the lab angle. Fission-fragment pulse-height spectra from the system O^{16} (165 MeV) + Au^{197} were observed at 140, 110, 90, 70, and 40 deg. The peak positions of these spectra plotted against the calculated energies constituted a calibration from 43 to 103 MeV (Fig. 3). Calculation of the lab energies is described in Appendix B.1.

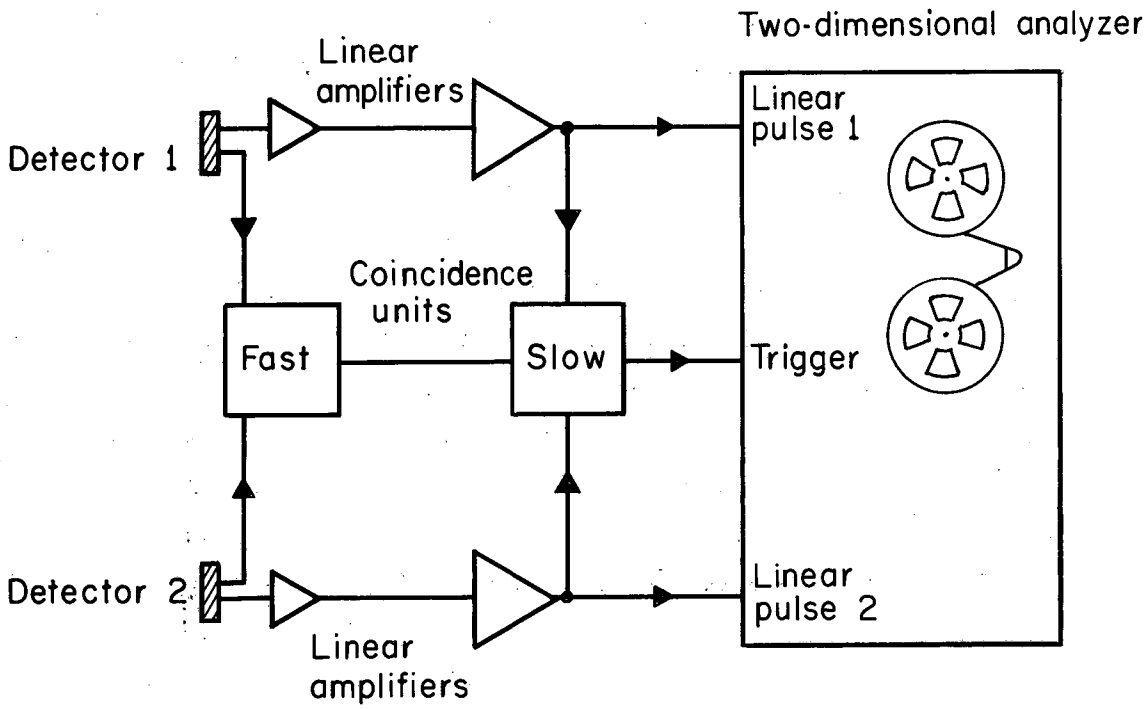

MU-27420

Fig. 2. Schematic diagram of the electronic system showing the linear amplifiers, coincidence units, and two-dimensional analyzer.

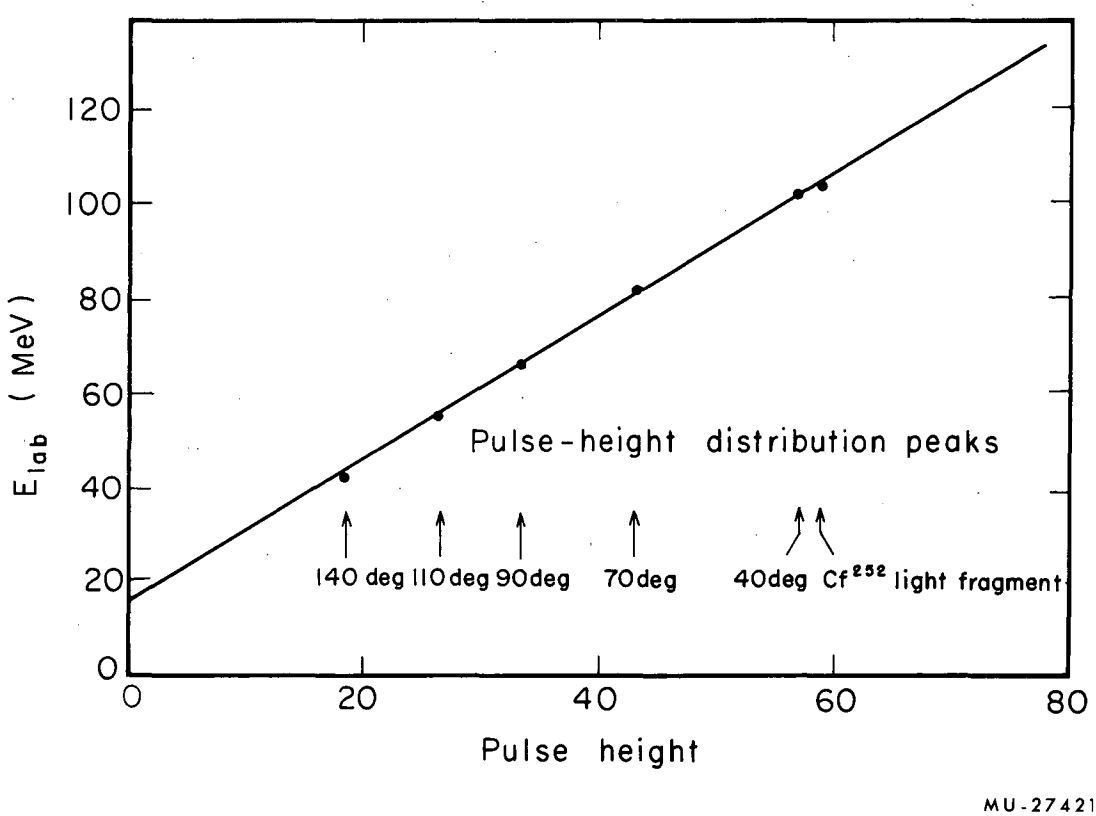

Fig. 3. Calibration of a linear system by using the angular variation of O^{16} (165 MeV) + Au^{197} fission-fragment energies. The Cf^{252} light fragment peak is also included.

2. Data Collection

Calculation of center-of-mass (c.m.) energies required a knowledge of the lab energies and one lab angle. Thus it was necessary to define the angle by collimating one detector. Collimation to an arc of 4 deg made the calculation fairly accurate, yet allowed a reasonable counting rate. This collimated detector was usually located at 90 deg (lab). The second detector had a sufficient width (20 deg) to accept all the fragments in coincidence with those striking the collimated detector.

The limiting factor in the data-collection rate was the counting rate in the larger detector. The intensities of the particle beams were adjusted to limit the overlapping of linear pulses from the larger detector to less than 2%. The counting rates were then about 10,000/min in the larger detector, 2,000/min in the collimated detector, and typically 500/min coincidence counts. When beam and target conditions were optimum, as many as 100,000 events were collected in a single experiment. With less favorable conditions, as few as 20,000 events were collected.

III. CALCULATIONS

In the following sections we shall discuss the conversion of the pulse heights to lab energies, and the transformations of the lab energies to c.m. energies, and to masses and total kinetic energies. The mass and total kinetic energy distributions are described in terms of their moments. One section is devoted to the errors in the experimental results.

A. Calculation of Laboratory Energies

The following operations and transformations were made by using the IBM 7090 computer.

The events stored sequentially on the magnetic tape were sorted according to pulse-height combination. This resulted in a three-dimensional surface with the pulse heights as two coordinates -V_1 and V_2 - and the number of events corresponding to each such combination as the third coordinate -$N(V_1, V_2)$. An example is given in Fig. 4. Such surfaces will be referred to as "contour maps", whether the first two coordinates are pulse height, energy, or mass.

The peak positions of the pulse-height spectra and their associated energies were analyzed by a least squares method to give the best fit to a straight line (see Fig. 3). Earlier attempts at fitting the data to a quadratic formula showed that no curvature term was needed. Similar data from the calibration of the two linear systems gave two sets of linear coefficients which were used to convert the pulse heights (V) to energies:

$$E'_{lab} = a + bV.$$

These energies were corrected for the energy lost in the target:

$$E_{lab} = E'_{lab} + \langle \Delta E \rangle .$$

The expression for $\langle \Delta E \rangle$ is derived in Appendix C.2.

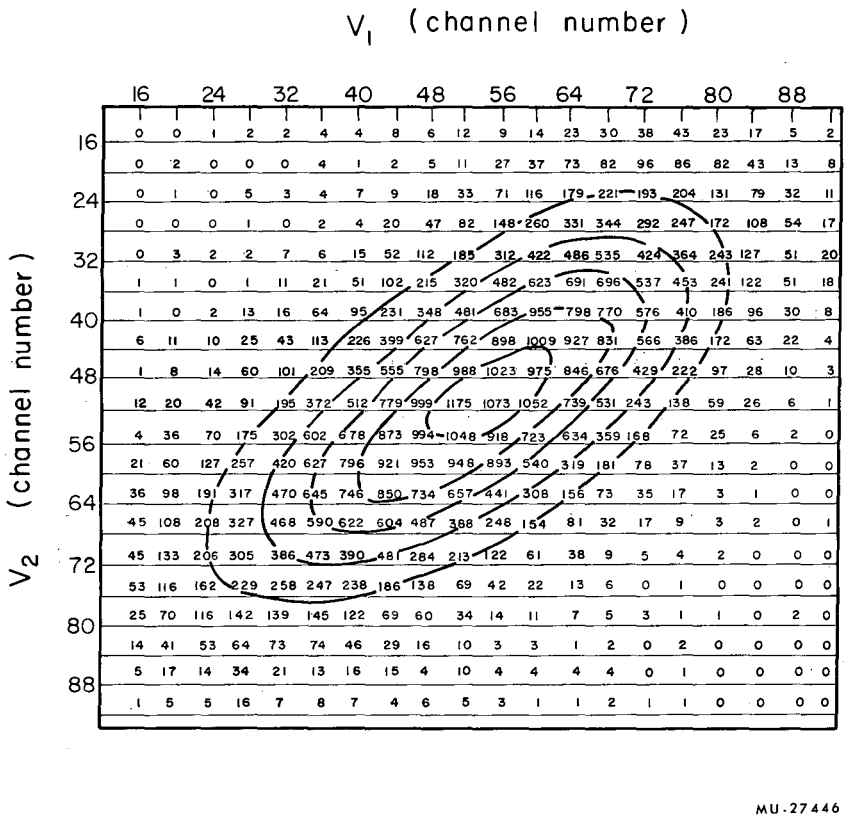

Fig. 4. "Contour map" for fragments from O^{16} (138 MeV) + U^{238}. The number of events plotted against V_1 and V_2 forms a "hill". Contours are at 200-event intervals.

B. Transformations

The two lab energies were then transformed into the c.m. system. Because the transformation equations were not explicit, an iterative approximation method was used in which the lab energies were introduced as the first approximation. The succesive approximations were required to converge on the final c.m. energy values to within 0.02 MeV. This proved to be a moderately fast and very accurate method. The details of this transformation method are given in Appendix B.2.

At this point a correction for detector "pulse-height defect" was made. One characteristic of this defect, for example, is that even when their energies are identical, different fragment masses give different pulse heights. For a detailed discussion, see Appendix C.4.

Each combination of c.m. energies has a unique total kinetic energy:

$$E_K = E_1 + E_2 .$$

Each combination also has a unique mass pair, which may be determined from the fact that the two fragments conserve linear momentum, p, in the c.m. system:

$$p_1^2 = p_2^2$$

$$A_1 E_1 = A_2 E_2$$

$$\frac{A_1}{A_2} + 1 = \frac{E_2}{E_1} + 1$$

$$\frac{A_2}{A_1 + A_2} = \frac{E_1}{E_1 + E_2}$$

$$\frac{A_2}{A_c} = \frac{E}{E_K}$$

Here A_c is the compound-nucleus mass, and E_K is defined above. The mass of the fragments in dimensionless units, A/A_c, ranges from zero to one, with distributions symmetric about one-half. An example of a transformation of lab energy coordinates into A/A_c and E_K coordinates is shown in Fig. 5.

Such a transformation to a new coordinate system requires not only the calculation of the new coordinates but also of the density of events in the new coordinates system. The method of density transformation used in these calculations is described in Appendix B.3. The lab energy contour maps were transformed into c.m. energy maps and mass-energy maps. Examples are given in Figs. 6 and 7. Figure 8 shows the mass-energy map as a series of mass distributions changing with total kinetic energy.

C. Moments in the Description of the Contour Maps

A contour map with coordinates A/A_c and E_K may be considered to be a series of mass distributions changing with total kinetic energy, as illustrated in Fig. 8. Or it may be thought of as a series of total-kinetic-energy distributions changing with mass. For all the distributions the mean, the second through the fourth central moments, and the coefficients of skewness and flatness were calculated.

For the mean, one can write

$$\langle x \rangle = \frac{\sum_i x_i \, N(x_i)}{\sum_i N(x_i)} .$$

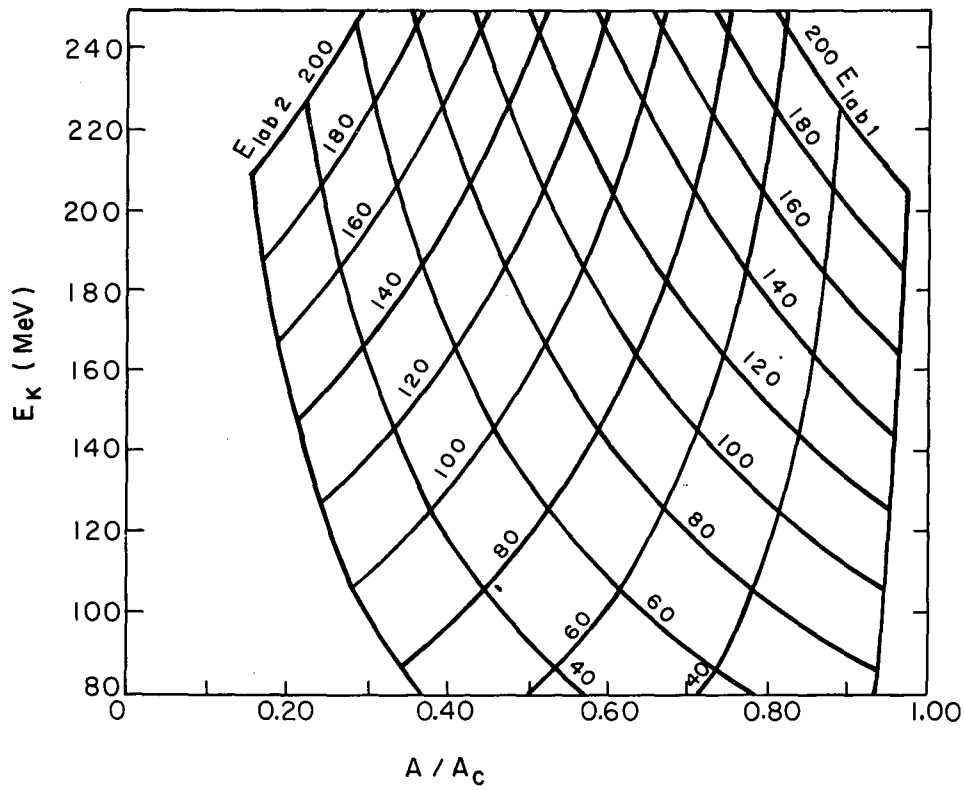

MU-27422

Fig. 5. Transformation of coordinates from laboratory energies to A/A_c and E_K for Ne^{22} (171 MeV) + Th^{232}.

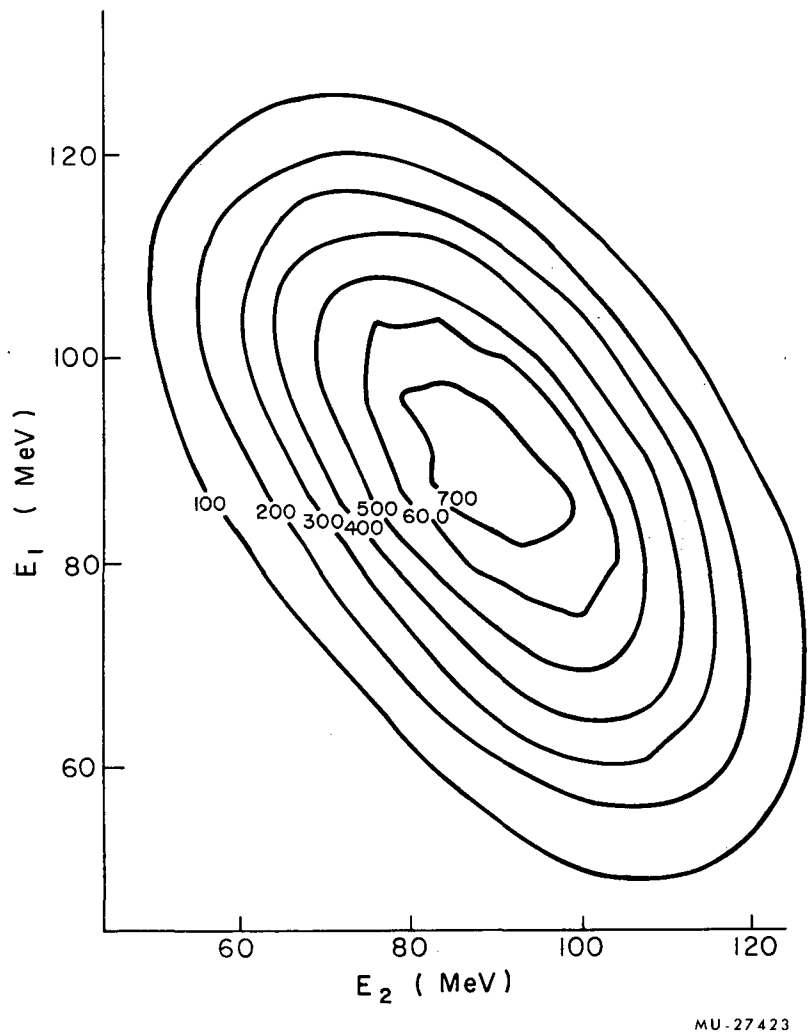

Fig. 6. Contour map in center-of-mass energy coordinates, E_1 and E_2, for O^{16} (138 MeV) + U^{238}. The contours are lines of constant $N(E_1, E_2)$.

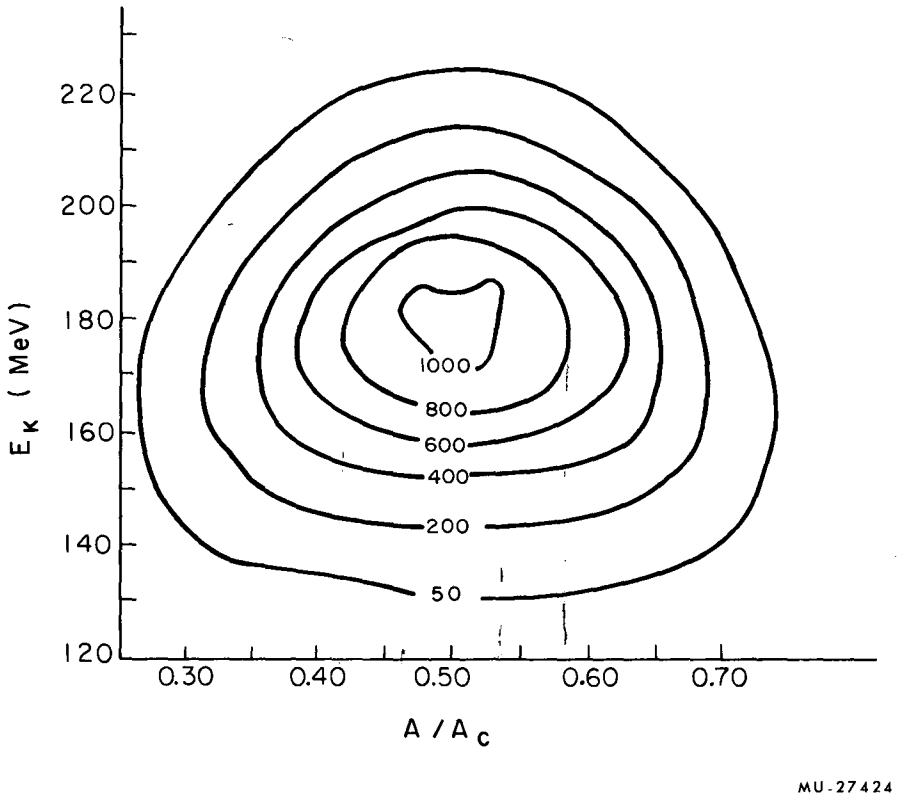

Fig. 7. Contour map in the coordinates A/A_c and E_K for O^{16} (138 MeV) + U^{28}.

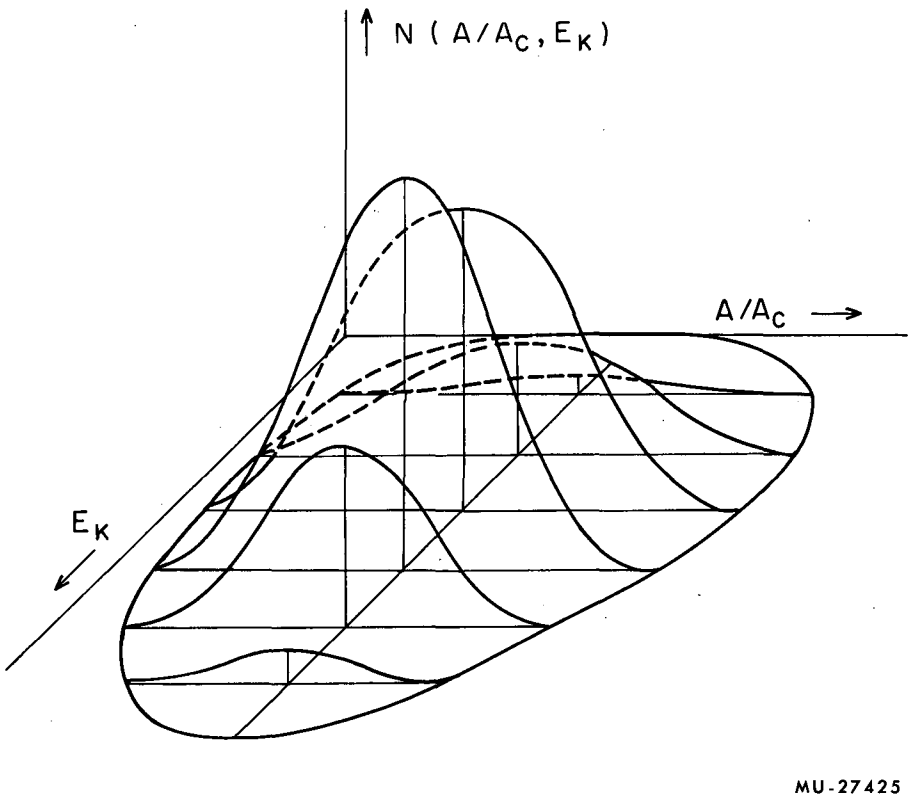

Fig. 8. Contour map for O^{16} (138 MeV) + U^{238} shown as mass distributions for various values of E_K .

For the central moments we have

$$\mu_r(x) = \frac{\sum_i (x_i - \langle x \rangle)^r N(x_i)}{\sum_i N(x_i)} ,$$

with $r = 2, 3,$ or $4,$ and where $N(x_i)$ is the number of events having $x = x_i$. The coefficients of skewness and flatness may be calculated from the central moments:

$$\alpha_3(x) = \mu_3(x)/[\mu_2(x)]^{2/3}$$

$$\alpha_4(x) = \mu_4(x)/[\mu_2(x)]^2 - 3.$$

Both are zero for a gaussian distribution. Details of the moments and their statistical errors are given in Appendix B.4.

D. Errors in the Mean and Variance of the Distributions

Two types of errors in the A/A_c and E_K distributions are discussed here: those affecting the mean, causing the distributions to shift, and those in the variance, causing widening of the distributions. Corrections for the mean energy loss in the target and for pulse-height defect were discussed briefly in the section on transformations. Still to be discussed are errors caused by electronic dispersion, effects of neutron emission on the mean and variance of the A/A_c and E_K distributions, and effects of target thickness and uncertainty of the defined angle on the variance of the distributions.

1. Dispersions from Detector and Electronic Sources

Amplifier noise and gain shifts cause dispersion of the single-fragment energy spectra. The dispersion caused by the electronic system was measured by a mercury pulser to be about 1/2%. However, it was not possible to measure the dispersion from the detectors, (no mono-energetic fission-fragment source was available). An indirect estimate of the overall detector and electronic dispersion (Section III.D.5.) suggests that this type of error is negligible. There is also some indication that the detector-amplifier combinations showed a higher gain when the heavy-ion beam was off than when it was on, and that the gain decreased with increasing beam intensity. Changes in beam intensity may thus have caused shifts in the pulse height during a particular period of data collection. Any such shift would have resulted in a spreading of the distributions.

2. Effects of Neutron Emission from the Fragments

For this discussion we shall assume that (a) no neutrons are emitted before the fission event (b) the neutrons emerge isotropically in the fragment's frame of reference,[8,9] and (c) the same number of neutrons emerge from each fragment. It follows that there is no change of the average velocity of a fragment, only a reduction of its mass resulting from the loss of neutrons. Therefore the average energy loss is proportional to the number of neutrons emitted. To a good approximation this has no effect on the mean of the mass distribution, because the numerator and denominator of A/A_c are reduced proportionately. However the mean of the E_K distributions are lowered in proportion to the average total number of neutrons lost in the events, $\bar{\nu}$:

$$\langle E_K \rangle_{\text{observed}} = \langle E_K \rangle \left(\frac{A_c - \bar{\nu}}{A_c} \right)$$

Distributions of mass and total kinetic energy are widened by neutron emission. This widening may be compared with the effects of poor resolution in a linear electronic system. Calculation of mass and total kinetic energy are based on the energies of the fragments immediately after the fission event, but the resolution of the prompt energy values is diminished when the fragments recoil from the random emission of several neutrons. Any quantity calculated from fragment energies after neutron emission necessarily has a wider distribution than the same quantity calculated from prompt energies. A detailed calculation and discussion of the effects of neutron emission appear in Appendix C.1.

3. Effects of Target Thickness

There is an uncertainty in the depth at which events occurred in the targets. Accordingly, the amount of energy lost by each fragment is uncertain. Only the average energy can be calculated. This results in decreased resolution just as in the case of neutron emission (see Appendix C.2).

4. Effects of the Uncertainty in the Defined Lab Angle

Analogously, because of the width of the collimated detector and the effective width of the target, there is an uncertainty in each fragment's emergent angle. Yet all the energies were transformed from the lab to the c.m. system on the assumption that the angle was well-defined. Again the uncertainty causes dispersion of the A/A_c and E_K distributions (see Appendix C.3).

5. Comparison of the Magnitude of the Dispersions

The dispersions caused by target thickness and uncertainty of the defined angle were found to be negligible when compared with those caused by neutron emission.

Comparison of radiochemical and electronic measurements of the mass distribution for the system C^{12} (119 MeV) + U^{238} indirectly showed the dispersion due to the detector and electronic systems to be negligible. The radiochemical measurement was taken to give the "intrinsic" distribution.[10] It's variance was $5.25 \times 10^{-3} (A/A_c)^2$. The variance

of the electronically measured distribution, $6.23 \times 10^{-3}\ (A/A_c)^2$, was corrected only for neutron dispersion. This corrected variance, $5.19 \times 10^{-3}\ (A/A_c)^2$ compares very well with the "intrinsic" variance. Therefore, the conclusion that only neutron emission caused observable errors in the variances of the distributions seems justified.

IV. RESULTS

The first column in Table I lists all the reactions studied. The kinetic energy and mass distributions are similar in all cases and have the general appearance of Fig. 8.

The most probable events are characterized by equal mass division and a kinetic energy of about 190 MeV. For mass divisions and kinetic energies deviating from the most probable values, the distributions fall off rapidly in a monotonic manner. Kinetic-energy distributions for a given mass division are bell-shaped, with average values and widths decreasing somewhat with increasing asymmetry of mass division. Mass distributions for a fixed kinetic energy are also bell-shaped but, with one exception, the widths of the mass distributions decrease markedly with increasing kinetic energy. We shall discuss this feature in detail.

Figure 9 shows the average kinetic energy for the reaction O^{16} (138 MeV) + U^{238}, as a function of mass asymmetry. The approximately parabolic decrease of the kinetic energy from a value of about 190 MeV at symmetry to 170 MeV at a mass fraction 0.7 is typical of all the cases studied.

Figure 10 shows the variance of the kinetic-energy distribution. The variance is almost constant except at extreme mass asymmetry, where it appears to drop off.

Figures 11 through 14 show the variance of the mass distribution as a function of the kinetic energy. We note that with the exception of the reaction O^{16} (103 MeV) + U^{238}, the variance (proportional to the <u>square</u> of the width of the mass distribution) decreases in a linear manner with increasing kinetic energy. A single straight-line relation seems to hold over the entire range of measurements from about 140 to about 220 MeV. In this interval the variance decreases by a factor of four. The slopes of these lines are given in Table I. The cases of O^{16} (103 MeV) + U^{238} constitutes a notable exception to

Table I. List of the reactions studied in these experiments, the excitation and rotational energies of the compound nuclei, and the slopes and intercepts, $\hat{E}_K$, of the plots of $\mu_2(A/A_c)$ vs E_K. The rotational energy is that of the spherical compound nucleus based on the maximum classical impact parameter.

Reaction	Excitation Energy (MeV)	Upper Limit of Rotational Energy (MeV)	Slope $[(A/A_c)^2(\text{MeV})^{-1}]$	$\hat{E}_K$ (MeV)
C^{12}(124 MeV)+Pu^{242}	92	11.2	-0.77×10^{-4}	249
O^{16}(165 MeV)+U^{238}	116	20.6	-1.00×10^{-4}	247
O^{16}(158 MeV)+U^{238}	110	18.8	-1.18×10^{-4}	247
O^{16}(141 MeV)+U^{238}	95	14.3	-1.04×10^{-4}	255
O^{16}(138 MeV)+U^{238}	92	13.5	-1.04×10^{-4}	248
O^{16}(138 MeV)+U^{238}[a]	92	13.5	-1.02×10^{-4}	255
O^{16}(129 MeV)+U^{238}	83	11.2	-1.08×10^{-4}	252
O^{16}(129 MeV)+U^{238}[a]	83	11.2	-0.77×10^{-4}	248
O^{16}(103 MeV)+U^{238}	58	4.3	----------	---
Ne^{22}(171 MeV)+Th^{232}	103	23.6	-1.01×10^{-4}	259
Ne^{22}(137 MeV)+Th^{232}	72	11.3	-0.93×10^{-4}	248

[a]Repeated experiments.

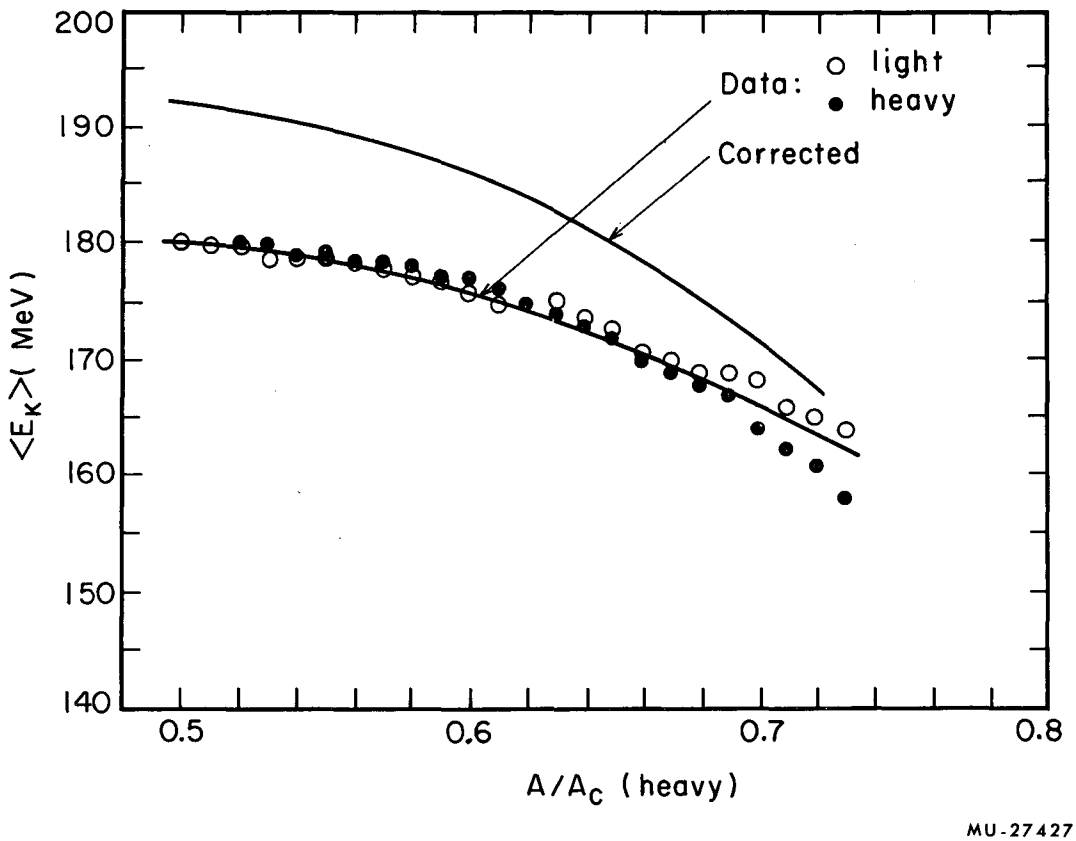

Fig. 9. Mean of the E_K distributions vs mass for O^{16} (138 MeV) + U^{238}. The upper curve shows the data corrected for the effects of neutron emission and energy loss in the target.

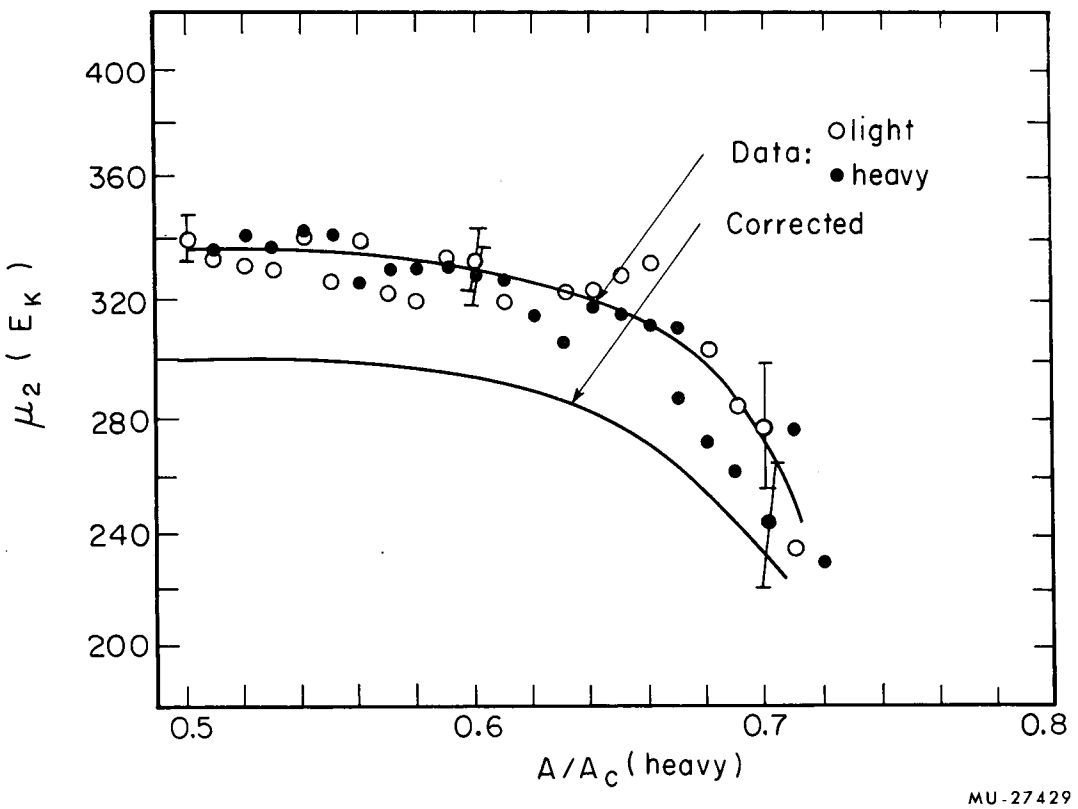

Fig. 10. Variance of the E_K distribution vs mass for O^{16} (138 MeV) + U^{238}. The lower curve shows the data corrected for the effects of neutron emission.

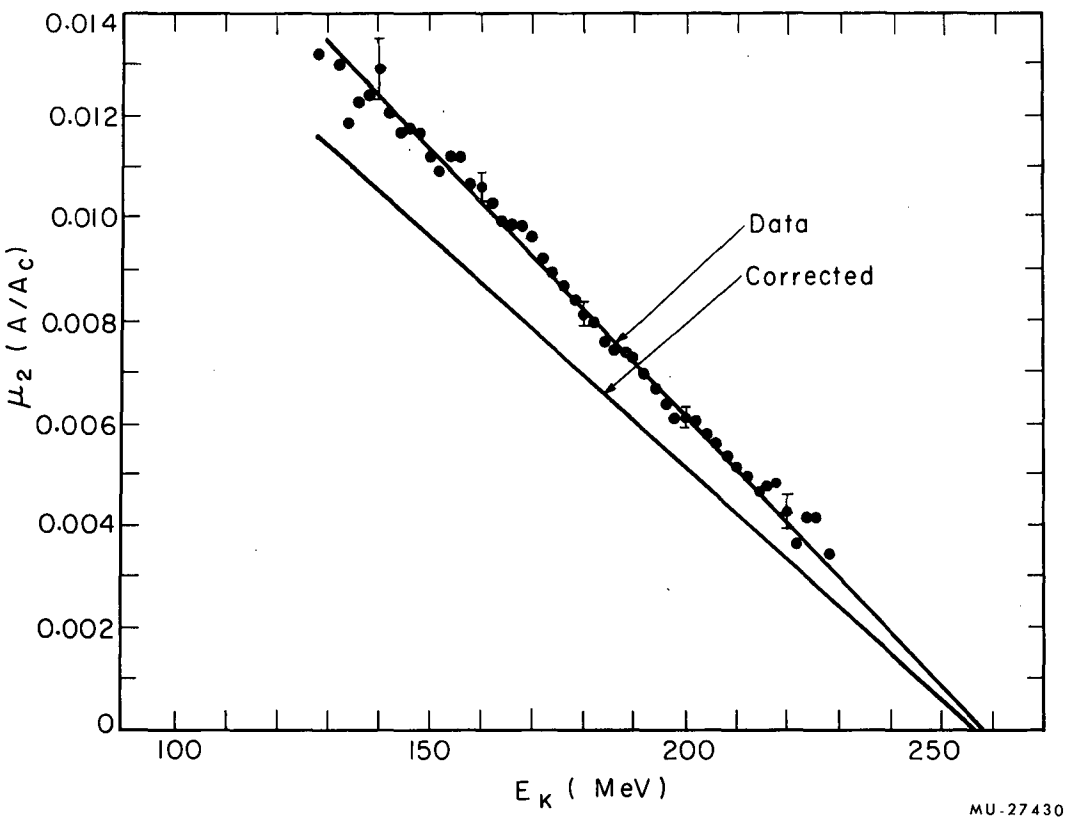

Fig. 11. Variance of the mass distribution vs E_K for O^{16} (138 MeV) + U^{238}. The lower curve shos the data corrected for the effects of neutron emission.

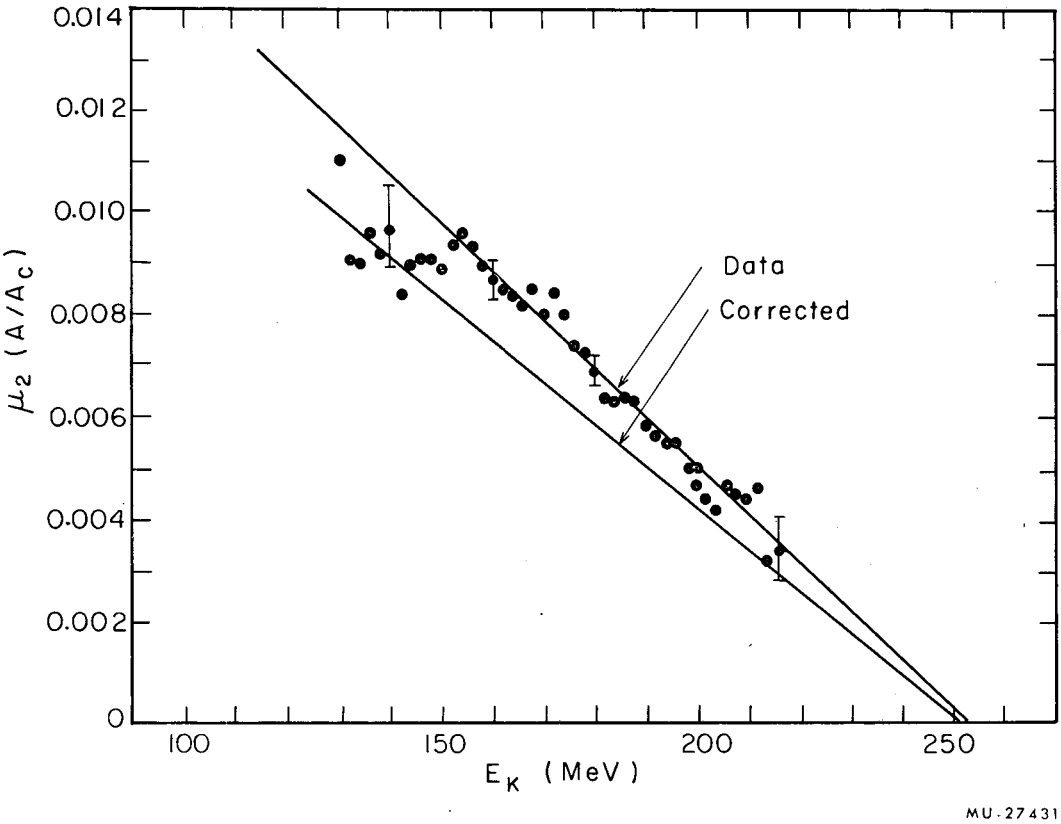

Fig. 12. Variance of the mass distribution vs E_K for Ne^{22} (137 MeV) + Th^{232}. The lower curve shows the data corrected for the effects of neutron emission.

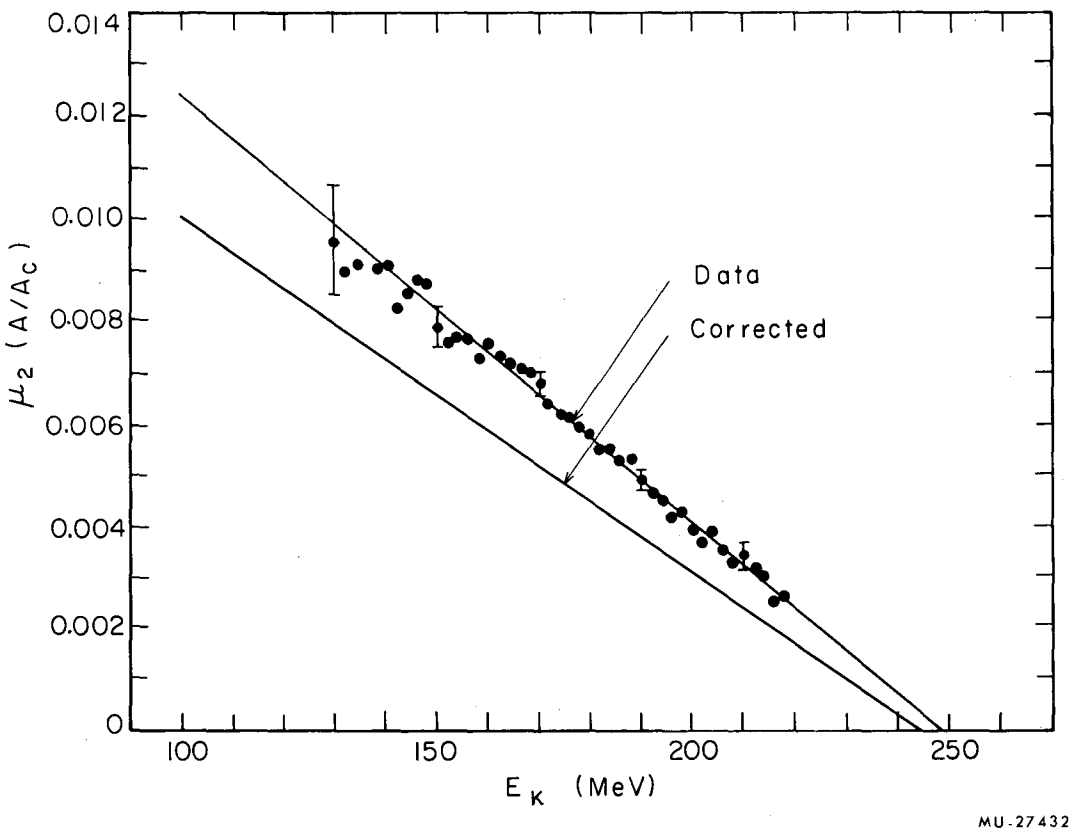

Fig. 13. Variance of the mass distribution vs E_K for (124 MeV) + Pu^{242}. The lower curve shows the data corrected for the effects of neutron emission.[12]

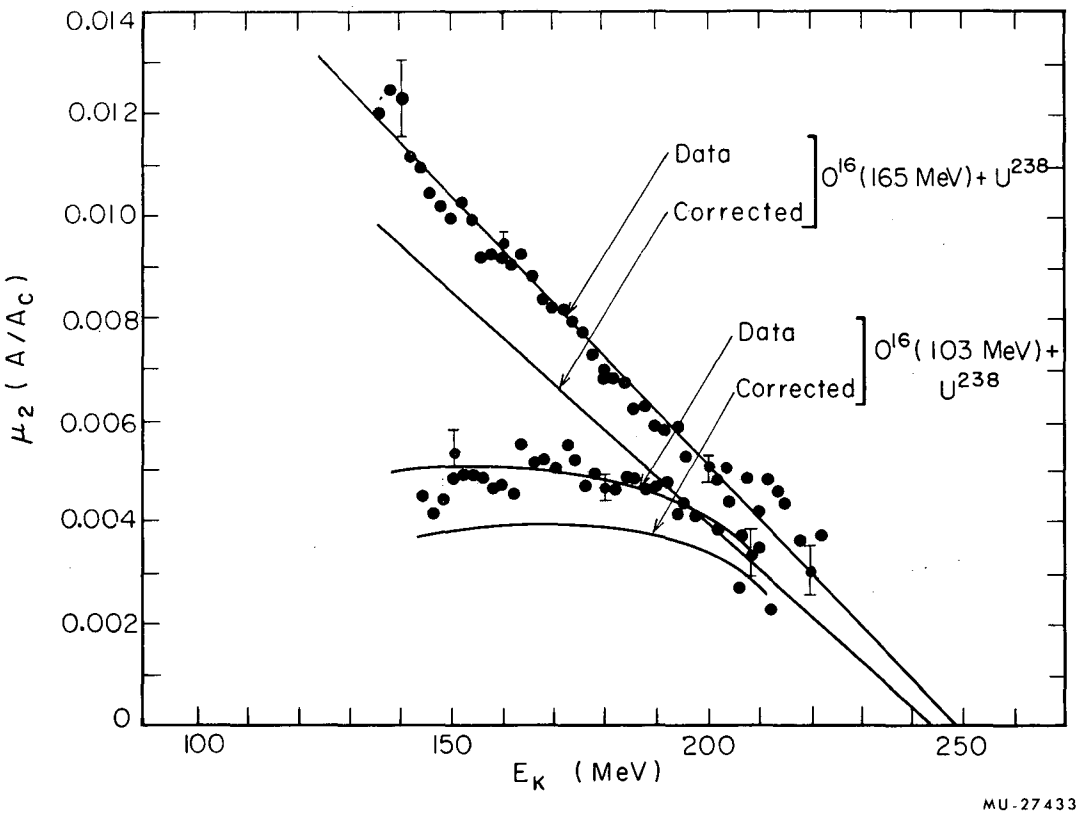

Fig. 14. Variance of the mass distributions vs E_K for the systems with highest and lowest excitation energies of these experiments (116 and 58 MeV). In each case the lower curve shows the data corrected for the effects of neutron emission.

the above behavior (Fig. 14). In this case the characteristic increase of the variance with decreasing kinetic energy does not hold below about 190 MeV. In fact, for low energies the variance appears to become independent of the energy.

In addition to the above overall features of the kinetic-energy and mass distribution, which will be discussed in the next section, further characteristics are revealed by a more detailed analysis of the data. The kinetic-energy distributions for fixed mass divisions are not quite symmetric about the average value, but leave a somewhat longer tail on the low-energy side. The mass distribution for a fixed kinetic energy are almost gaussian at the highest kinetic energy, but become gradually more nearly rectangular with decreasing energy. Figure 15 gives a quantative description of this effect.

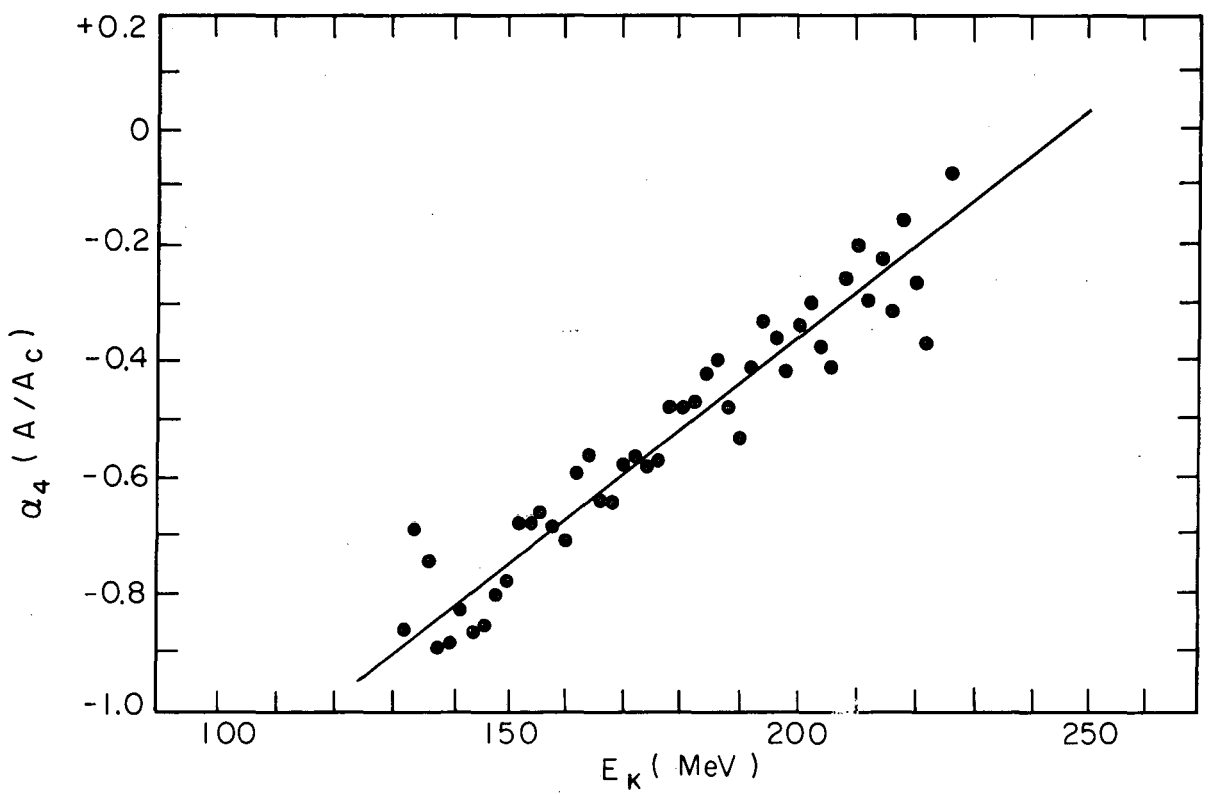

Fig. 15. Coefficient of flatness of the mass distributions vs E_K for O^{16} (138 MeV) + U^{238}. The lower the value of α_4, the more rectangular the distribution. For a gaussian distribution, α_4 equals zero.

V. DISCUSSION

A. Kinetic Energy Distributions

An approximately parabolic decrease of the average kinetic energy with increasing asymmetry of mass divisions, as found in Fig. 9, is in line with simple estimates of the electrostatic repulsion, Z_1Z_2e/L, between two fragments at constant or almost constant separation L.

Figure 16 shows a comparison of a typical experimental curve with a calculation in which L was taken as constant. (The value of L was chosen to normalize the results at symmetry). The lower curve refers to the case where the charge-to-mass ratios of the fragments are the same as for the original nucleus. Thus we have

$$E_K = Z_1Z_2e^2/L = (A_1 \cdot A_2)\left[\left(\frac{Z_c}{A_c}\right)^2 \quad \frac{e^2}{L}\right].$$

The upper curve illustrates the effect of allowing the charge-to-mass ratios in the two fragments to readjust themselves slightly, namely to those values that minimize the potential energy of the two fragments at the separation L.[11] The result is that the charge in the narrow β-stability parabola of the light fragment is moved toward the most stable charge. This causes the charge in the wider parabola of the heavy fragment to be moved away from the most stable charge. The process results in an increase in the interaction energy, but the net effect on the estimated value of E_K is quite small--from zero at symmetry to 3 MeV at $A/A_c = 0.7$.

We note that in either case the curves corresponding to a calculation with a constant value of L fall below the experimental curve by about 5% at $A/A_c = 0.7$. For the calculation to reproduce the experiments, L would have to decrease gradually with asymmetry, the change amounting to 5% at $A/A_c = 0.7$.

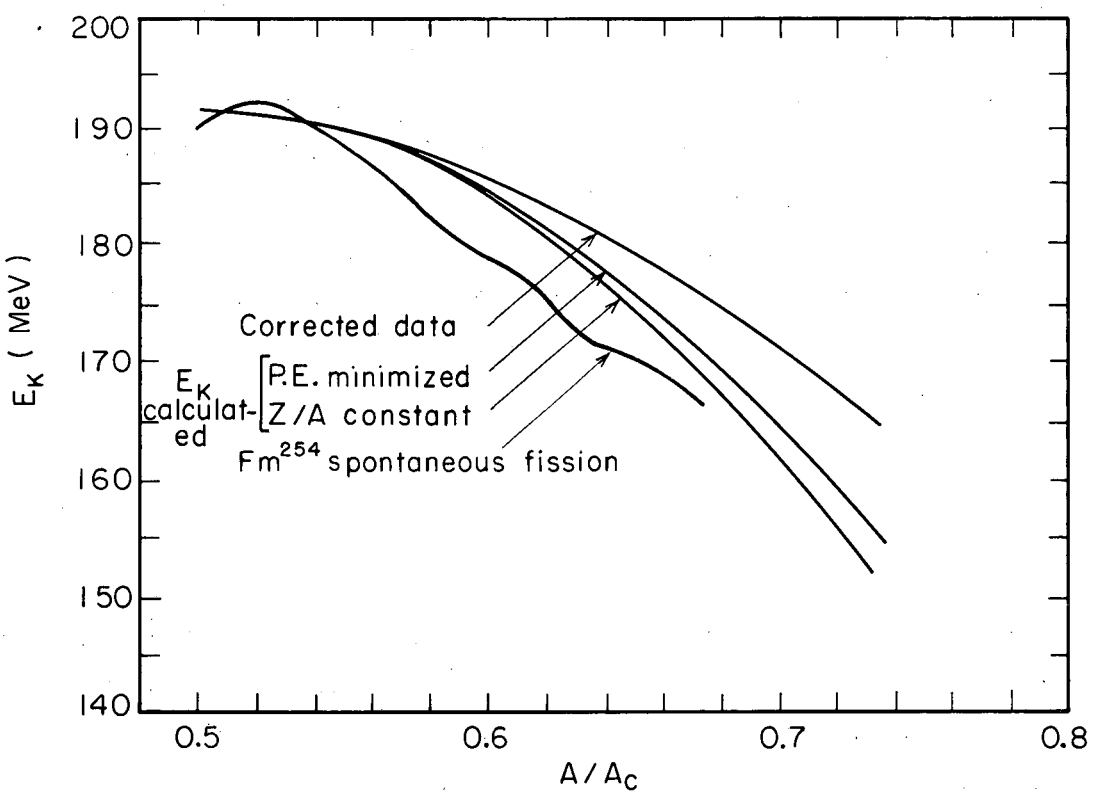

Fig. 16. Mean value of E_K as a function of A/A_c for O^{16} (138 MeV) + U^{238} showing the neutron corrected data. The two calculations of E_K as Coulomb repulsion are included for comparison. The mean kinetic energy for the spontaneous fission of Fm^{254} is also included.

Britt has recently analyzed the kinetic energies of fragments from the fission of elements in the Pb-U region at moderate excitation energies (up to about 20 MeV).[12] The results are in general more complicated than in our case. They were interpreted by Britt in terms of two processes--two "modes" of fission--each with its characteristic, almost constant charge separation L.

Figure 16 compares one of our results with Brandt's recent measurements[13] on the spontaneous fission of Fm^{254}. The average kinetic energies are 188 and 189 MeV, respectively. The behavior of the kinetic energy as a function of asymmetry is more complicated in the case of spontaneous fission, a feature common to low-excitation-energy fission.[12,14]

The average kinetic energy of 188 MeV is also close to the value of 185 MeV found by Sikkeland and Viola[15] in the reaction $O^{16} + U^{238}$.

Our measurements of the variance of the kinetic-energy distribution (See Fig. 10) suggest a decrease at extreme asymmetry. Such a decrease may be looked upon as a loss of freedom of the fissioning nucleus to choose its effective separation of charges at scission. A decrease of the variance of a variable may be a general feature of a shortage of available energy associated with extreme values of another variable. A very pronounced decrease in a variance which may be attributed to this cause is evident in the case of the mass distributions, which we shall discuss in the next section.

B. Mass Distributions

The systematic decrease of the variance of the mass distributions, illustrated in Figs. 11-14, may be associated with the loss of freedom of the fissioning nucleus to choose its asymmetry (at the moment of scission), as the restriction imposed by the requirement of a higher kinetic energy becomes more and more severe.[16] In the case of O^{16} (103 MeV) + U^{238},

whose excitation energy is 58 MeV, the freedom to choose asymmetry does not continue to increase with decreasing kinetic energy (See Fig. 14). Because this was the only deviating case studied, we will not discuss it further than to point out the possible association between the rather constant restriction on the asymmetry at low kinetic energies and the relatively low excitation energy.

Since the maximum energy available for fission is always limited, an extreme situation would be realized in those cases where all the available energy was required to appear as kinetic energy. In such cases (where relative frequency would be increasingly small) there would be no energy left for deviations of any other variables from their optimum values (i.e. those values associated with the maximum energy release). Consequently the variances of all distributions, including in particular the mass-division variable, would tend to zero as the kinetic energy approaches a certain upper limit. More generally, at any given kinetic energy it is possible to write an upper limit, required by conservation of energy, on the value of any variable. We shall illustrate this in the case of the mass-division variable A/A_c. Figure 17 shows a plot of the energy release for Fm^{254} as a function of A/A_c. According to the liquid-drop formula, used in this illustration, the maximum energy release E_{max} = 230MeV occurs for symmetric fission, and in the spontaneous fission of such a liquid drop, only strictly symmetric divisions would be energetically possible for events characterized by a kinetic energy release of E_K = 230MeV. Figure 17 shows that the range of asymmetries available energetically for a kinetic energy E_K smaller than this upper limit would be (approximately) proportional to the square root of $(E_{max} - E_K)$. In other words, the square of the maximum width of a mass-division distribution should be approximately a straight line in a plot against E_K. This is illustrated in Fig. 18.

We may compare this result with the empirical findings in Figs. 11-14 that the variance of the mass distributions--equal to the square of the rms widths--depends linearly on E_K. The slopes of the experimental lines are listed in Table I, as are the intercepts $\hat{E}_K$. All ten

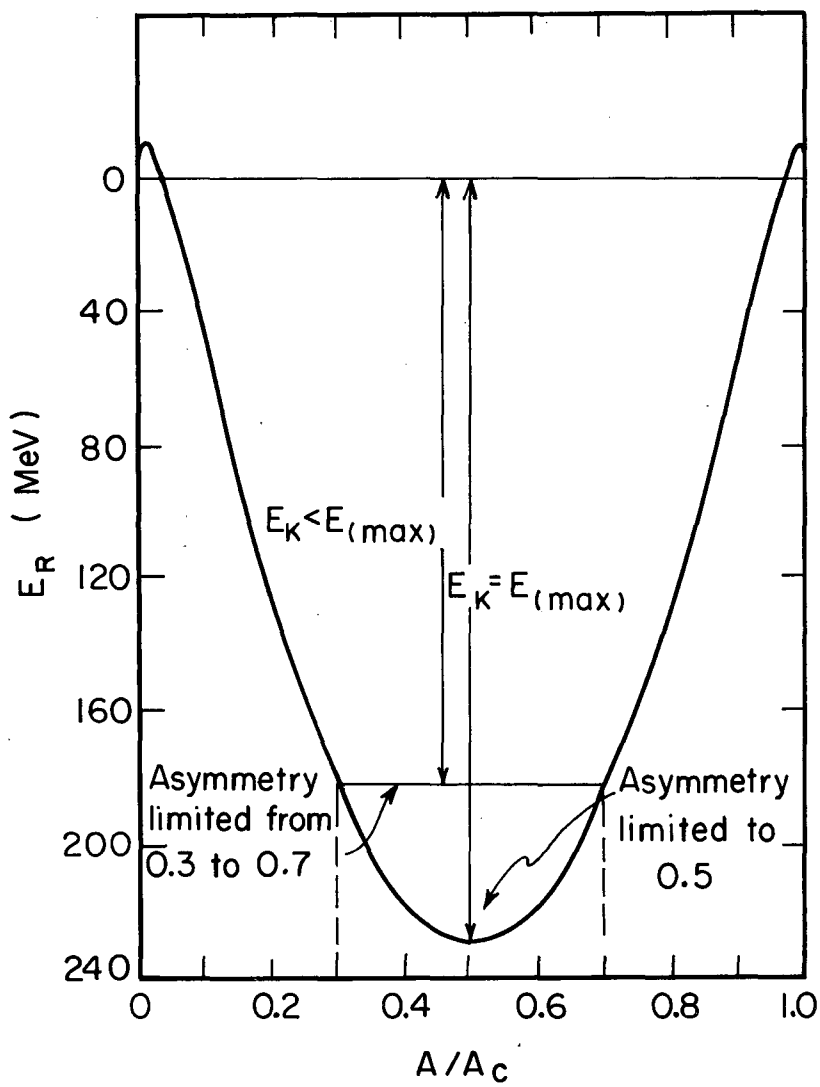

MU-27439

Fig. 17. Energy release as a function of mass for the spontaneous fission of Fm^{254}, illustrating the limits placed on the mass asymmetry for different E_K. The curve is based on the constant-charge-ratio hypothesis.

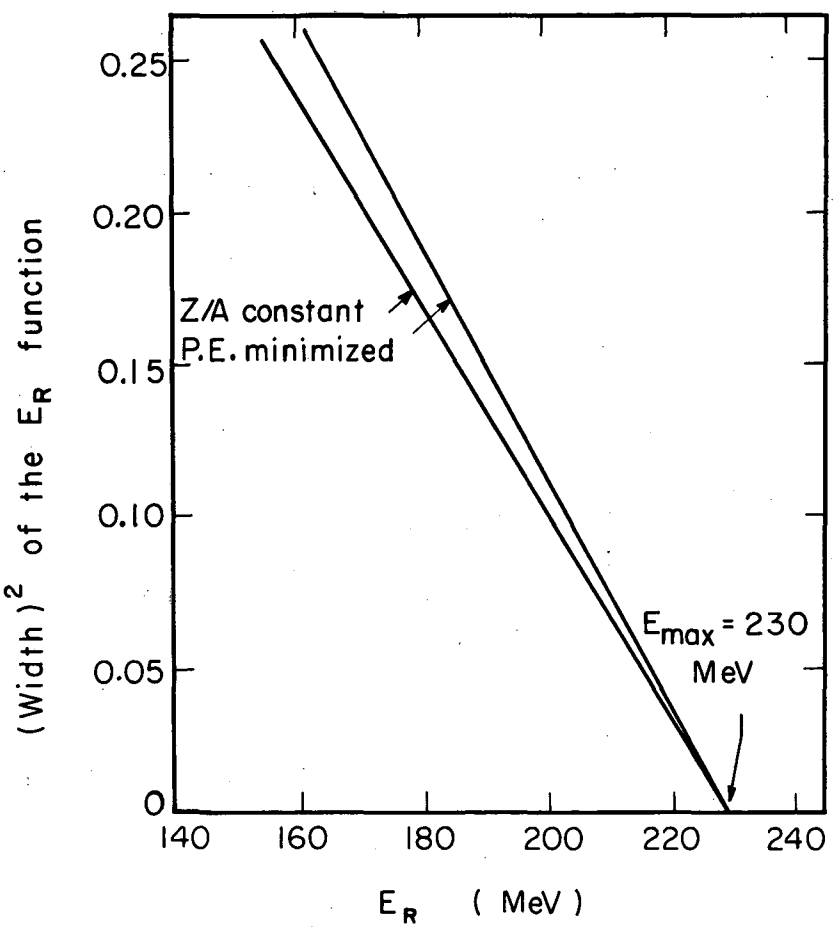

MU-27440

Fig. 18. The square of the width of the energy-release function, $(1 - 2A/A_c)^2$, vs energy release for Fm^{254}.

observed slopes are similar, and the intercepts are all quite close to 252 MeV (the average is 252±4 MeV). We have noted that in the spontaneous fission of Fm^{254} the maximum energy release available is estimated to be of the order of 230 MeV. This estimate is subject to some uncertainities. If the special stability of the two symmetric fragments with each other is taken into account, (according to Cameron's masses) 243 MeV is found for the energy release. We may also point out that 252 MeV is equal to the potential energy of two equal spherical fragments whose centers are separated by 14.3 fermis, which corresponds to almost tangent spheres. Although this may have a deeper significance, we have not been able to find a convincing argument why the variance of the mass division coordinate should tend to zero at kinetic energies corresponding to this particular configuration. The experimental value of about 252 MeV for the intercepts is near the maximum energy release. Although the intercept appears to be somewhat higher than the maximum energy release, there is of course no violation of energy conservation, since in the case of induced fission the total amount of energy available is much higher than 230 or 240 MeV. In our case, the total energy available may be in fact higher, making E_{total} between 290 and 340 MeV. That the intercept $\hat{E}_K$ comes out closer to the energy release than to the total energy is in line with the expectation that most of the extra energy, being in the form of internal excitation, is not easily available for conversion into kinetic energy of the fragments.

Estimating how much excitation energy is actually present in the nucleus at the moment of fission is in general difficult. We would like to conclude this discussion with a consideration of the factors that would tend to make the relevant excitation energy different from that obtained from the Q value of the reaction.

C. Remarks Concerning the Excitation Energy

In some cases the heavy ion breaks apart and deposit only a fraction of its mass in the target nucleus. This leads to the formation of an excited nucleus which has not only a lower excitation energy, but also a lower mass and charge than the expected compound nucleus. If the resulting nucleus is a very heavy one, it will usually have sufficient energy to fission. Thus events involving compound-nucleus formation may be mixed with fission events from nuclei of uncertain mass, charge, and excitation energy.

However, the linear velocities of the excited nuclei resulting from breakup reactions are lower than those of nuclei formed by the capture of the entire heavy ion. This forward velocity is given to the fission fragments. The two fragments from a low-velocity event (corresponding to breakup-induced fission) emerge in the laboratory system separated by larger angles than do two fragments from a high-velocity event (corresponding to heavy-ion-induced fission). This has been graphically illustrated by Sikkeland et al.[17] In the cases of the maximum energies of the heavy ions (10 MeV per nucleon) there is a large difference in the angles between the fission fragments produced by the two reactions. If the detectors are located to detect fragments from compound-nucleus fission essentially no fragments from breakup-induced fission are detected. However at lower bombarding energies there is a smaller difference in the angles between fragments produced in the two cases. Thus at lower bombarding energies a larger fraction of the observed fragments will come from breakup-induced fission. This fraction is estimated to be 5% for the reaction O^{16} (138 MeV) + U^{238}.

However, we may compare the results of two experiments, one in which the observed fragments came only from compound-nucleus fission, the other in which some of the fragments also came from fission following a breakup reaction. Figure 11 shows a plot of $\mu_2(A/A_c)$ vs E_K of the fragments for the reaction O^{16} (138 MeV) + U^{238}. Approximately 5% of the observed fragments came from breakup reactions. A comparison with

a similar plot for the reaction O^{16} (165 MeV) + U^{238} (Fig. 14) reveals no apparent difference in shape. The slopes and intercepts are also not significantly different (Table I). We may conclude that inclusion of some events of unknown initial mass, charge, and excitation energies, has not significantly affected the widths of the distributions represented by μ_2 (A/A_c) vs E_K.

In the case of the compound-nucleus reactions we must consider the distribution of total energy between excitation and rotation. We must also consider how much energy appeared in the form of neutrons before fission occurred. The calculated maximum rotational energies for spherical compound nuclei are listed in Table I for each case studied. These energies are calculated assuming a spherical projectile colliding at a point just tangent to a spherical target. Such a collision gives the maximum rotational energy, which is probably more than twice the average energy. Thus in the reaction with the highest rotational energy studied here, namely Ne^{22} (171 MeV) + Th^{232}, the average rotational energy is estimated to be about 10 MeV. During the fission process even this energy may be lower, because the moment of inertia becomes larger with increased distortion. In any event, even in this extreme case, the average rotational energy is less than or about 10% of the initial energy of the compound nucleus.

Angular momentum and rotational energy play an important role in the probability of partial de-excitation of the compound nucleus by neutron emission. Hiskes has shown that the fission barrier is lowered by large angular momentum.[18] Pik-Pichak has shown that the barrier for neutron emission is increased by high angular momentum.[19] A study of the available experimental data by Vandenbosch and Huizenga showed that for 1 MeV decrease in the difference between the fission threshold and the neutron binding energy the average value of Γ_n/Γ_f decreases by an order of magnitude.[20] The average experimental values of Γ_n/Γ_f for the reactions Cf^{252} $(\alpha, 4n)$ Fm^{252} and U^{238} $(O^{16}, 4n)$ Fm^{250} are ~0.25 and ~0.07, respectively.[21,22] Although the excitation energies of comparable compound nuclei produced in our experiments with heavy ions were larger, the correspondingly increased angular

momenta should have reduced the effective values of Γ_n/Γ_f still further. De-excitation by neutron emission would therefore seem to be negligible. However it should be emphasized that the conclusions of the experiments do not depend to any important degree on the validity of the arguments concerning the extent of de-excitation.

VI. APPENDICES

A. Some Experimental Details

1. Electronic System

The electronic system was designed and used to measure and store the two pulse heights corresponding to both fragment kinetic energies for a large number of binary-fission events (Fig. 19). The coincidence system made certain that the measured pulse heights came from a single event. The two linear systems amplified the pulses from the semiconductor detectors, and finally the pulse heights were measured and recorded by the two-dimensional analyzer.

a. Linear systems. Each linear system consisted of the detector, a Model VI preamplifier, and a Model VI linear amplifier in its double-delay-line mode.[23] The n-type side of the detector diode, to which the positive bias was applied, supplied a negative pulse to the preamplifier through a 52-Ω coaxial cable. The signal from the preamplifier passed from the bombardment area to the linear amplifier in the counting area through an impedance-matched 185-Ω cable. The White cathode-follower output of the linear amplifier was connected to the input of the two-dimensional analyzer by a 185-Ω cable. Another cathode-follower output supplying the variable-delay and-gate unit was also used for peripheral monitoring of the pulses by an oscilloscope or a separate pulse-height analyzer.

b. Coincidence system. The p-type side of the surface-barrier detector was grounded through a small inductor consisting of a ferrite core with five hand-wound turns. The fast rise time of the pulse was observed at the juncture of the detector and the inductor. This 1- to 5-mV positive pulse passed from the chamber to an inverting distributed amplifier, then to a series of noninverting distributed amplifiers,[24] one in the bombardment area and two in the counting area. There the transistorized coincidence unit clipped the input pulses from the two systems to 10^{-8} sec.[25] In case of a coincidence event, the coincidence unit put out a 1/2-V negative pulse which was amplified by another inverting amplifier,

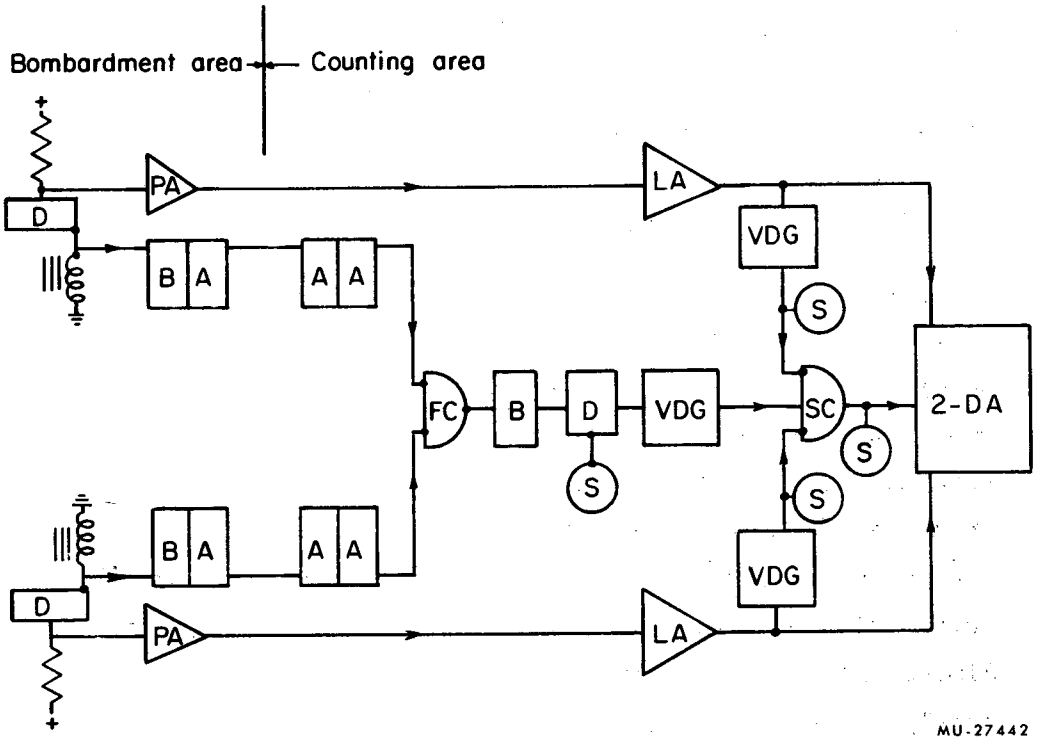

Fig. 19. Electronic system. The n-type side of the detectors is connected to the positive bias. The components include (D) 150-Ω-cm surface-barrier detector,[5] (PA) Model-VI preamplifiers, (LA) Model-VI linear amplifiers, (B) HP-460B inverting distributed amplifers, (A) HP-460A noninverting distributed amplifiers, (FC) a fast coincidence unit, (D) a 10-Mc discriminator, (VDG) variable-delay-and-gate units, (SC) a slow-coincidence unit, (S) scalers, and (2-DA) a two-dimensional analyzer.

then passed to a 10-Mc discriminator-scaler.[26] Up to this point, high-impedance cables and careful impedance matching were required.

The fast coincidence and slow linear systems were then brought together. Slow coincidence ($\sim 10^{-6}$ sec) by itself did not have sufficient time resolution to prevent large numbers of accidentals. The fast system ($\sim 10^{-8}$ sec) was prone to produce short trains of noise pulses. Coupling them reduced both the accidentals and the noise to negligible levels. Pusles from the 10-Mc discriminator and pulses from the linear amplifiers (cathode-follower output) were passed into three variable-delay-and-gate units. These units gave out square pulses whose length and delay could be adjusted so that, in case of a real fission event, the three appeared in concert. These square pulses were collected in a slow coincidence unit. The output from this unit activated the two-dimensional analyzer.

c. Two-dimensional analyzer. The first portion of the two-dimensional analyzer consisted of two Penco analog-to-digital converters. On receiving a coincidence pulse from the slow coincidence unit, the converters were activated. They measured the heights of the pulses arriving from the linear systems at that moment, and gave out pulse trains, the number of pulses being proportional to the pulse heights. These trains were counted by two scalers, whose contents were then stored in two consecutive positions of a small magnetic-core memory. Twenty such events filled the memory. The twentieth activated the magnetic-tape transport unit which received the contents of the memory. The memory was then cleared for further data collection.

2. Preparation of targets

The Pu^{242}, U^{238}, and Th^{232} target materials were deposited on nickel foils 135 $\mu g/cm^2$ thick. Such foils are commercially available with thick copper backings. Foils were spot-welded between two flat annuli made of stainless steel (dimensions: outer diameter, 1 in.; inner diameter 1/2 in.; thickness, 1/64 in.). The copper backing of the exposed portion of the foil was dissolved in a $K_2Cr_2O_7$-H_2SO_4 solution, and the entire assembly carefully washed and dried.

For electrodeposition of Pu^{242} a mounted foil was held horizontally by a clamp which also served as an electrical contact.[13] The end of a platinum wire, to be used as an anode, was lowered to within 1/16 in. of the center of the foil. Ten μl of saturated NH_4Cl containing 100 μg of 98.5% isotopically pure Pu^{242} were touched to the platinum wire and allowed to slide down to contact the horizontal nickel foil. This formed a cone of solution, with the base of the cone on the foil and the apex at the platinum wire. A 4-V potential was applied for 15 min. The solution was neutralized with 10 μl of concentrated NH_4OH before the potential was removed. The area covered was small and the material not very uniform. Yields ranged from 40 to 70%.

Before electrodeposition of the Th^{232}, the annuli of the foil assembly were coated with quick-drying varnish to make them electrically insulating. The mounted foil was then immersed vertically into 25 ml of conductivity water containing 200 to 300 μg of Th^{232} in its nitrate form. Platinum anodes were suspended one on each side of the target, and a 10-V potential applied for 1 hr. The result was a moderately even coating of Th^{232} oxide on both sides of the Ni foil. Yields ranged from 80 to 95%.

The U^{238} targets (natural uranium) were prepared by vaporization of UF_4 onto the mounted nickel foil. The UF_4 on a molybdenum "boat" filament (to be heated by an electric current) and the mounted foil were placed under a bell jar and the bell jar was evacuated. Two collimators were used to minimize the heating of the foil: the first hid the boat, except the section containing UF_4, from the foil; the second limited the exposed area of the foil. Very gradual heating and cooling of the boat was necessary to keep the foil from breaking. The thickness of the uranium was estimated by the color during the vaporization process; a steel-blue color indicated a thickness of about 100 $\mu g/cm^2$.

Gold targets were commercial 1/4-mil foils spot-welded between two annuli.

B. Data Processing

1. Calculation of E_{lab} for the Calibration

The calibration of the linear systems used a comparison of pulse heights with the calculated lab energies for fission fragments observed at several different angles (Section II B.1). The calculation of E_{lab} as a function of angle for O^{16} (165 MeV) + Au^{197} fission fragments is taken up here.

Consider a compound nucleus with a velocity in the lab system, v_{cl}, which emits a fission fragment at a c.m. angle θ with velocity v_{fc} (Fig. 20). In the lab system it will be observed at an angle ψ with a velocity v_{fl}. According to the law of cosines, we have

$$v_{fl}^2 = v_{fc}^2 + v_{cl}^2 - 2v_{fc}v_{cl}\,(\pi-\theta).$$

We define the transformation parameter:

$$x = \frac{v_{cl}}{v_{fc}} .$$

Then we can write

$$\frac{E_{lab}}{E_{c.m.}} = \frac{v_{fl}^2}{v_{fc}^2} = 1 + x^2 + 2\,x\cos\theta .$$

In order to find the value of $\cos\theta$ we use the law of sines:

$$\frac{\sin\psi}{v_{fc}} = \frac{\sin(\theta - \psi)}{v_{cl}} = \frac{\sin\theta\cos\psi - \cos\theta\,\sin\psi}{v_{cl}}$$

and

$$x = \sin\theta\,\cot\psi - \cos\theta .$$

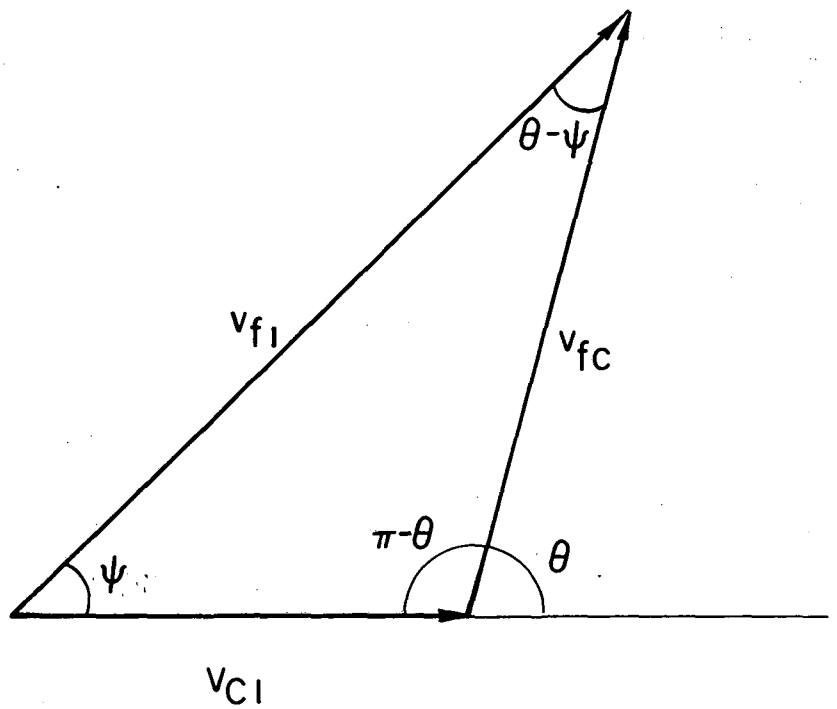

MU-27443

Fig. 20. Velocity diagram indicating the velocities of a fragment in the lab and c.m. systems and the associated angles.

Writing $\sin\theta$ in terms of $\cos\theta$ in order to solve for $\cos\theta$, we obtain

$$\cos\theta = -x \sin^2 \psi \pm \cos\psi \, (1 - x^2 \sin^2\psi)^{1/2} .$$

Only the positive sign has physical significance.

For the calculations of E_{lab}, for O^{16} (165 MeV) + Au^{197}, $E_{c.m.}$ was taken to have a value of 75 MeV.[17] The peaks of the fragment energy distributions were taken to represent symmetric fission; x^2 was thus calculated for symmetric fission:

$$x^2 = \frac{A_p E_p}{2 A_c E_{c.m.}} = 0.077 ,$$

where p refers to the projectile, and c to the compound nucleus. For this expression, the prompt rather than the post-neutron c.m. energy was required. The prompt energy in MeV was calculated from

$$E_{c.m.} \text{ (prompt)} = 75 \frac{A_c}{A_c - \bar{\nu}}$$

where $\bar{\nu}$ is the average number of neutrons. The value of $\bar{\nu}$ calculated from Leachman's formula[27] was taken to be 14.6. After these energies were corrected for energy loss in the gold target (Appendix C.2), they were compared with pulse-height spectra to calibrate the linear systems.

2. Transformation of E_{lab} to $E_{c.m.}$

Calculation of the two c.m. energies requires that both lab energies and one lab angle be known. Because the equation is not explicit, an iterative method was used which depends on the lab energies as the first approximation. The method appears as a subroutine in the program for computing the transformations.

First the transformation parameters were approximated from the lab energies (here the lab energies are referred to as E_1 and E_2):

$$x_1^2 = \frac{A_p E_p}{A_c (E_1 + E_2)} \cdot \frac{E_2}{E_1}$$

$$x_2^2 = \frac{A_p E_p}{A_c (E_1 + E_2)} \cdot \frac{E_1}{E_2} ,$$

where the subscript p refers to the projectile, and c to the compound nucleus. Then the cosine of one c.m. angle was calculated from the known lab angle:

$$\cos\theta_1 = -x_1 \sin^2\psi_1 + \cos\psi_1 (1-x_1^2 \sin^2\psi_1)^{1/2} .$$

Using $\theta_2 = \pi-\theta$, we calculated the c.m. energies:

$$E_1 = E_{lab\ 1} / (1 + x_1^2 + 2x_1 \cos\theta_1)$$

$$E_2 = E_{lab\ 2} / (1 + x_2^2 - 2x_2 \cos\theta_1) .$$

These energies were then introduced as a second approximation into the transformation parameter equations, and the process was repeated.

Successive approximations were continued until both energies agreed with their previous approximations to within 0.02 MeV. Four to six iterations were normally needed. For some cases with very small lab energies, the successive approximations oscillated, converged on zero, or even diverged. In case of oscillation or divergence, the process was stopped after 40 iterations and the lab energies recorded.

3. Transformation of the Density of Events

Transformation to a new coordinate system requires not only finding the new coordinates, but also finding the density of events in the new coordinate system. The method of density transformation used in these experiments is illustrated in Fig. 21. For the sake of explanation only let us suppose that the actual grid size of the lab-energy contour map is 20 MeV on each side, as pictured. (In the actual transformations the grid size was much smaller.) Also suppose the grid size of the mass-energy map is 0.10 and 20 MeV, respectively, as shown. The mass-energy point associated with the 80-120 MeV lab energies would fall between 0.40 and 0.50 on the mass scale and between 180 and 200 MeV on the energy scale. The number of events, N(80 MeV, 120 MeV), would then be divided. The largest fraction would go to the nearest mass-energy point (0.50, 180 MeV); the points (0.40, 180 MeV) and (0.50, 200 MeV) would receive approximately equal fractions and the smallest fraction would be given to the farthest point (0.40, 200 MeV).

In a similar treatment of the lab-energy combination (60 MeV, 120 MeV), the fraction of the events going to (0.50, 180 MeV) in the mass-energy system would be very small. Moderate fraction of the events with lab-energy combinations (80 MeV, 100 MeV) and (100 MeV, 100 MeV) would also go to the mass-energy point (0.50, 180 MeV). The sum of these fractions would be taken as the number of events having $A/A_c = 0.50$ and $E_K = 180$ MeV.

For the purposes of the above explanation, the grid size of the lab energy map has been taken to be 20 by 20 MeV; 0.10 A/A_c by 20 MeV has been taken for the grid size of the mass-energy map. Actually the grid sizes were 2- by 2-MeV and 0.01-A/A_c by 2-MeV respectively.

4. The Moments[28] and their Statistical Errors[29]

Let us define the rth moment of a distribution of the parameter x:

$$m_r = \frac{\sum_i x_i^r N(x_i)}{m_0} ,$$

where $m_0 = \sum_i N(x_i)$, and $N(x_i)$ is the number of times that $x = x_i$.

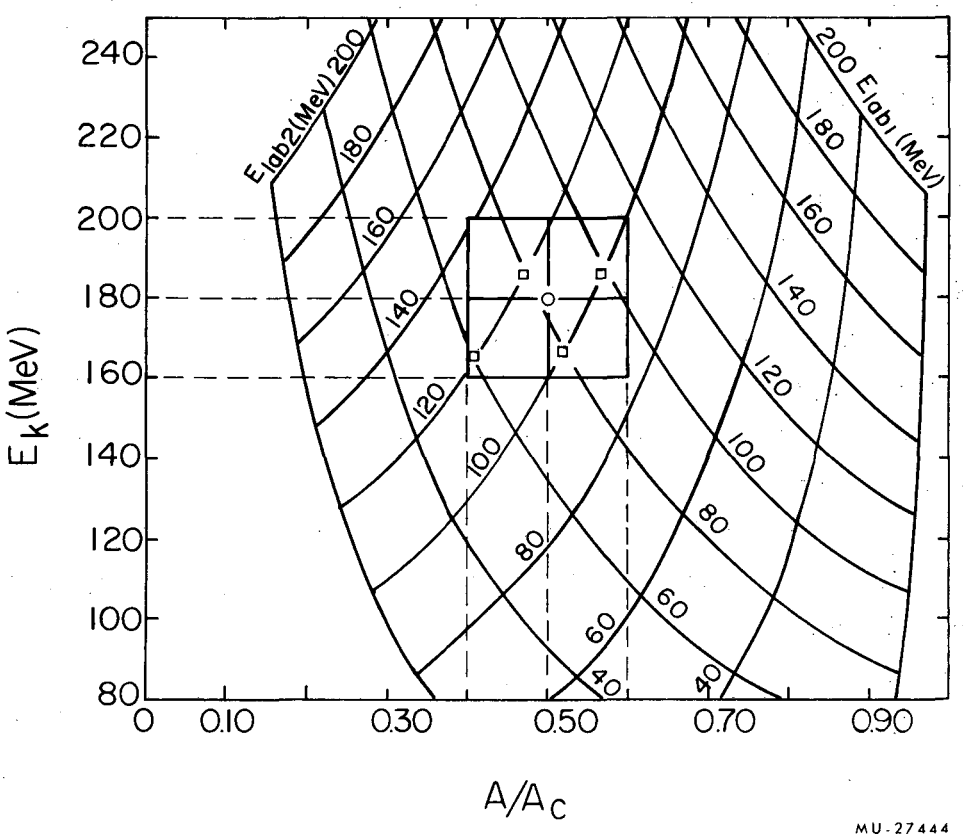

Fig. 21. Plot of lab energies on mass-energy coordinates, illustrating the transformation of the density of events.

Let us define the rth central moment by

$$\mu_r = \frac{\sum_i (x_i - m_1)^r N(x_i)}{m_o} .$$

The moments, m_r , are easily computed numerically, although the central moments, μ_r , are not. Therefore the central moments were calculated as expansions in terms of the moments:

$$\mu_2 = m_2 - m_1^2$$

$$\mu_3 = m_3 - 3m_2 m_1 + 2m_1^3$$

$$\mu_4 = m_4 - 4m_3 m_1 + 6m_2 m_1^2 - 3m_1^4 .$$

The mean of the distribution is identically the first moment:

$$\langle x \rangle = m_1 .$$

The second central moment is the variance. Its square root is the rms width of a distribution. The third and fourth central moments were used to calculate the dimensionless coefficients of skewness and flatness,

$$\alpha_3 = \mu_3/(\mu_2)^{3/2} ,$$

and

$$\alpha_4 = (\mu_4/\mu_2^2) - 3 ,$$

respectively. Both would be zero if the distribution were gaussian. Thus, a positive coefficient of skewness would imply that the distribution had a "tail" at values higher than the mean, and dropped off more quickly at values below the peak. A positive coefficient of flatness would imply that the distribution was more peaked than a gaussian, while a negative value would imply a tendency toward a flat top.

The statistical errors in the mean and variance were determined from the moments.[29] For clarity, let us redefine $N(x_i) \equiv f_i$. Then we may write the first moment as

$$m_1 = \frac{\sum x_i f_i}{m_0} .$$

If we differentiate with respect to the jth term, we find

$$\frac{\partial m_1}{\partial f_j} = \frac{x_j}{m_0} - \frac{\sum x_i f_i}{m_0^{\,2}} = \frac{(x_j - m_1)}{m_0} .$$

Because the error in f_j, δf_j, is the statistical error due to counting the events having values of x between x_j and $x_j + \Delta x$, we have

$$(\delta f_j)^2 = f_j$$

$$(\delta m_1)^2 = \frac{\sum (x_j - m_1)^2 f_j}{m_0} = \frac{\mu_2}{m_0} .$$

Similarly, for the variance we have

$$\mu_2 = \frac{\sum (x_i - m_1)^2 f_i}{m_0} ,$$

$$\frac{\partial \mu_2}{\partial f_j} = \frac{m_0 (x_j - m_1)^2 - \sum (x_1 - m)^2 f_i}{m_0^{\ 2}} ,$$

$$= \frac{1}{m_0} \left[(x_j - m_1)^2 - \mu_2 \right]$$

$$(\delta \mu_2)^2 = \sum \left[\left(\frac{(x_j - m_1)^2 - \mu_2}{m_0} \right) \delta f_j \right]^2 .$$

Again we can write

$$(\delta f_j)^2 = f_j$$

$$(\delta \mu_2)^2 = \frac{1}{m_o} \left[\frac{\sum (x_j - m_1)^4 f_j}{m_0} - \mu_2^{\ 2} \frac{\sum f_j}{m_0} \right]$$

$$(\delta \mu_2)^2 = \frac{1}{m_0} (\mu_4 - \mu_2^{\ 2}) .$$

C. Corrections

If an observed quantity, x_0, is the sum of an intrinsic quantity, x, and an error in its measurement, δx, then a distribution of x_0 will have a mean:

$$\langle x_0 \rangle = \langle x \rangle + \langle \delta x \rangle$$

and a variance

$$\mu_2 (x_0) = \mu_2 (x) + \mu_2 (\delta x) + 2\mu_2 (x, \delta x).$$

The variance was defined in Appendix B.4. The last term in the above expression is the covariance, defined as

$$\mu_2 (x, \delta x) = \langle x\delta x \rangle - \langle x \rangle \langle \delta x \rangle.$$

If the error in the measurement of x is independent of the value of x, the covariance is zero. The errors considered in the first three following sections are largely independent of the values of the quantities being measured. The mean and variance of the intrinsic distribution are thus taken to be

$$\langle x \rangle = \langle x_0 \rangle - \langle \delta x \rangle$$

and

$$\mu_2(x) = \mu_2 (x_0) - \mu_2 (\delta x) .$$

Thus only the mean value and variance of the error distribution are considered.

1. Effects of Neutron Emission on the Mass and Total-Kinetic- Energy Distributions[30]

We assume the following regarding neutron emission:

(a) All neutrons emitted in a fission event come from excited fragments.

(b) The neutrons emerge isotropically from each fragment.[8,9]

(c) The energy of a neutron is not correlated with that of its predecessor.

(d) The same number of neutrons come from each fragment.

a. Effects on mass distributions. The masses were calculated according to the equation

$$A_2/A_c = E_1/E_K .$$

We wish to study mass distributions as a function of E_K. Thus the error in the mass for a given E_K is

$$\frac{\delta A_2}{A_C} = \frac{\delta E_1}{E_K} .$$

The variance of the error distribution is

$$\mu_2\left(\frac{\delta A_2}{A_c}\right) = \frac{1}{E_K^2} \quad \mu_2 \quad (\delta E_1)$$

where δE_1 is any error in the energy of one fragment.

What has been said thus far applies to all types of dispersion. In this case, the dispersion is caused by the emission of a series of neutrons; each neutron adds to the dispersion. Because of the assumptions of isotropic emission and uncorrelated energies, the variance of the distribution may be written as the sum of the variance for the single-

neutron error distributions. Thus we have

$$\mu_2 \left(\frac{\delta A}{A_c} \right) = \frac{1}{E_K^2} \sum_{i=1}^{\bar{\nu}_1} \mu_2 (\delta E) = \frac{\bar{\nu}}{2E_K^2} \mu_2 (\delta E),$$

where $\bar{\nu}_1 = \bar{\nu}/2$ is the average number of neutrons lost from each fragment, and δE is the change in energy of that fragment caused by the emission of one neutron. Then we must determine (1) $\mu_2 (\delta E)$, the variance of the error distribution caused by the emission of a single neutron, and (2) $\bar{\nu}$ as a function of the kinetic energy and the excitation energy. The approach taken here is similar to some extent to that taken by Terrell.[30]

A fragment with velocity v_f emits a neutron with velocity v_c at θ in the fragment's frame of reference (Fig. 22). The resulting fragment's velocity, v_f^*, may be written

$$v_f^{*2} = v_f^2 + \left(v_c \frac{m}{A^*}\right)^2 - 2 v_f v_c \frac{m}{A^*} \cos\theta ,$$

where m is the neutron mass and A^* is the resulting fragment's mass. Multiplying through by $A^*/2 = (A-1)/2$ and taking the initial energy term to the left side, we find:

$$\delta E = E^* - E = - \frac{E}{A} + \frac{m}{A^*} E_c - 2 \left(E_c \, m \frac{E}{A}\right)^{1/2} \cos\theta ,$$

where E_c is the c.m. energy of the neutron.
The variance of a distribution in δE may be written

$$\mu_2 (\delta E) = \langle \delta E^2 \rangle - \langle \delta E \rangle^2.$$

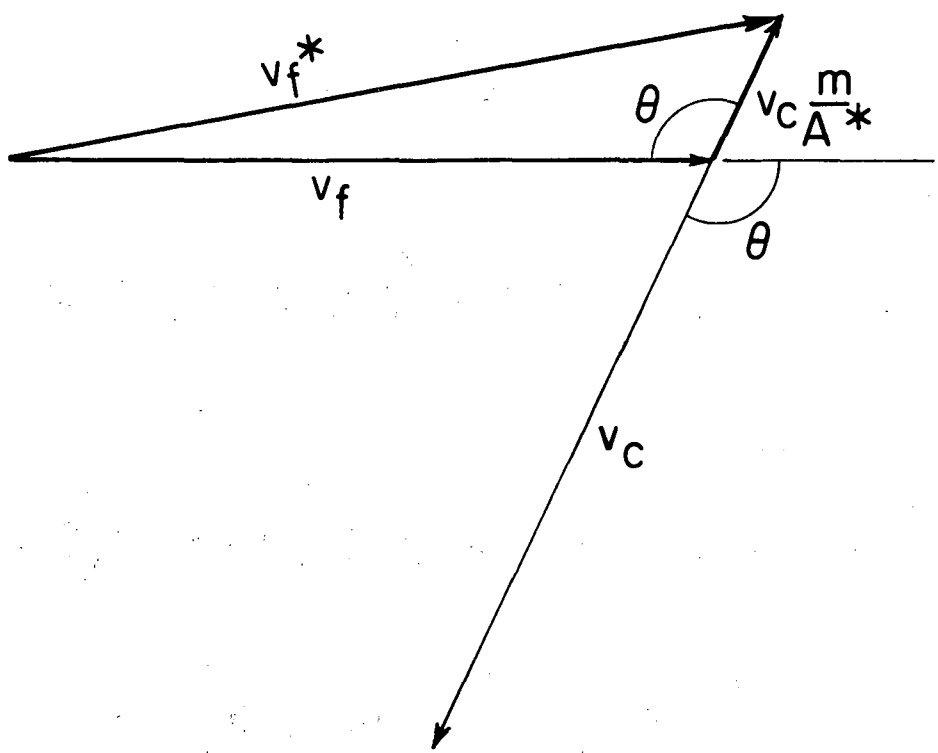

MU-27445

Fig. 22. Effect of neutron evaporation on a fragment's velocity. The fragment's initial velocity was v_f ; it had a velocity v_f^* after emitting a neutron at θ with velocity v_c.

Thus we need the quantities

$$\langle \delta E^2 \rangle = \left\langle \left(\frac{E}{A} \right)^2 \right\rangle + m^2 \langle E_c \rangle \frac{1}{A^2} + 4m \langle E_c \rangle \frac{E}{A} \langle \cos^2\theta \rangle$$

$$- 2m \langle E_c \rangle \left\langle \frac{E}{A} \cdot \frac{1}{A^*} \right\rangle$$

and

$$\langle \delta E \rangle^2 = \left\langle \frac{E}{A} \right\rangle^2 - 2m \langle E_c \rangle \left\langle \frac{E}{A} \right\rangle \left\langle \frac{1}{A^*} \right\rangle + m^2 \left\langle \frac{1}{A^*} \right\rangle^2 \langle E_c \rangle^2 .$$

It follows that

$$\mu^2(\delta E) = \mu_2\left(\frac{E}{A} \right) - 2m \langle E_c \rangle \mu_2\left(\frac{E}{A}, \frac{1}{A^*} \right) + 4 m \langle E_c \rangle \left\langle \frac{E}{A} \right\rangle \langle \cos^2 \theta \rangle$$

$$+ m^2 \left[\langle E_c^2 \rangle \left\langle \frac{1}{A^{*2}} \right\rangle - \langle E_c \rangle^2 \left\langle \frac{1}{A^*} \right\rangle^2 \right] .$$

We may make the following simplifications. For isotropic emission we have

$$\langle \cos^2\theta \rangle = 1/3 .$$

If the energy distribution of the neutrons in the fragment's moving system follows the expression,[9] $N(E) \propto E/T^2 \, e^{-E/T}$, then we have

$$\langle E_c^2 \rangle = \frac{3}{2} \langle E_c \rangle^2 .$$

Rewriting the energy per nucleon of the fragment as

$$\frac{E}{A} = \frac{E_K}{A_c}\left(\frac{A_c}{A} - 1\right)$$

we find

$$\mu_2\left(\frac{E}{A}\right) = \frac{E_K^2}{A_c^2}\ \mu_2\left(\frac{A_c}{A}\right) .$$

Similarly we have

$$\mu_2\left(\frac{E}{A}\ ,\ \frac{1}{A^*}\right) \cong \frac{E_K}{A_c^{\,2}}\ \mu_2\left(\frac{A_c}{A}\right) .$$

The variance of the energy-error distribution may now be written as

$$\mu_2\,(\delta E) = \frac{E_K^2}{A_c^2}\ \mu_2\left(\frac{A_c}{A}\right) - 2m\,\langle E_c\rangle\ \frac{E_K}{A_c^2}\ \mu_2\left(\frac{A_c}{A}\right)$$

$$+\ \frac{4}{3}\ m\,\langle E_c\rangle\ \frac{E_K}{A_c}\left[\left\langle\frac{A_c}{A}\right\rangle - 1\right]$$

$$+\ \frac{m^2}{A_c^2}\ \langle E_c\rangle^2\left[\frac{1}{2}\left\langle\left(\frac{A_c}{A}\right)^2\right\rangle + \mu_2\left(\frac{A_c}{A}\right)\right] .$$

Examination of the four terms in this equation shows that the second and fourth terms are about two orders of magnitude smaller than the third. Eliminating these as negligible, we have

$$\mu_2(\delta E) = \frac{E_K^2}{A_c^2}\,\mu_2\left(\frac{A_c}{A}\right) + \frac{4}{3}\,\frac{E_K}{A_c}\,m\,\langle E_c\rangle\left[\left\langle\frac{A_c}{A}\right\rangle - 1\right].$$

We may take $\left\langle\frac{A_c}{A}\right\rangle$ to be two. If we expand the inverse of A/A_c about its mean value in a Taylor's expansion, and take only the first two terms, we obtain

$$\frac{A_c}{A} = \left\langle\frac{A_c}{A}\right\rangle - \left(\frac{A}{A_c} - \left\langle\frac{A}{A_c}\right\rangle\right)\left\langle\frac{A_c}{A}\right\rangle^2 ;$$

then the variance of A_c/A is approximately

$$\mu_2\left(\frac{A_c}{A}\right) = \left\langle\frac{A_c}{A}\right\rangle^4 \mu_2\left(\frac{A}{A_c}\right) = 16\,\mu_2\left(\frac{A}{A_c}\right).$$

This may be expressed in terms of E_K as

$$\mu_2 \left(\frac{A}{A_c} \right) = - 1.24 \times 10^{-4} E_K ,$$

because , as we saw experimentally, the two are related by a straight line. The variance of the energy-error distribution may now be written

$$\mu_2 (\delta E) = \frac{4}{3} \frac{E_K}{A_c} m \langle E_c \rangle - 2.0 \times 10^{-3} \frac{E_K^3}{A_c^2} .$$

The mean value of the neutron energy, $\langle E_c \rangle$, was estimated to be 2.3 MeV.[9] This value was assumed to apply for all fragment masses and excitation energies.

It remains only to determine $\bar{\nu}$ from

$$\bar{\nu} = \frac{\langle E_R \rangle + E_X - E_K}{\langle E_B \rangle + \langle E_c \rangle} - 1 ,$$

where $\langle E_R \rangle$ is the mean energy released in an event, E_X is the initial compound-nucleus excitation, and $\langle E_B \rangle$ is the mean binding energy of a neutron in this range of fragment masses, 6.0 MeV. Both $\langle E_R \rangle$ and $\langle E_B \rangle$ were found from Cameron's mass formula.[31] The -1 term results because not all the excitation energy can be expended in neutron emission. Late in an evaporation chain, a nucleus no longer has enough energy to evaporate another neutron. The energy remainder, if assumed to be distributed evenly from zero to $\langle E_B \rangle + \langle E_c \rangle$,has an average value $(\langle E_B \rangle + \langle E_c \rangle)/2$. Thus, on the average, the number of neutrons evaporated from a fragment is one-half neutron less than the nonintegral number calculated; one neutron less for both fragments. However experiments indicate that this number should be greater than one.[14] Rearranging, we find:

$$\bar{\nu} = \left(\frac{\langle E_R \rangle - E_K}{6.0 + 2.3} - 1 \right) + \frac{E_X}{6.0 + 2.3} .$$

For $E_K = 190$ MeV, this becomes

$$\bar{\nu} = 3.7 + 0.12\, E_X .$$

This corresponds very well with Leachman's formula[27]

$$\bar{\nu} = \bar{\nu}_0 + 0.12\, E_X ,$$

where $\bar{\nu}_0$ is 4.0 for Fm^{254}.[32]

The entire expression for the variance of the mass-error distribution due to neutron emission becomes

$$\mu_2 \left(\frac{\delta A}{A_c} \right) = \frac{\bar{\nu}}{2} \frac{\mu_2 \ (\delta E)}{E_K^{\ 2}}$$

$$= \frac{1}{2} \left(\frac{229 + E_X - E_K}{8.3} - 1 \right) \left(\frac{4}{3} \frac{m\, E_c}{E_K\, A_c} - 0.002 \frac{E_K}{A_c^{\ 2}} \right)$$

To indicate the magnitude of the dispersion, we take the case of O^{16} (138 MeV) + U^{238}, finding

$$\mu_2 \left(\frac{\delta A}{A_c}\right) = \frac{14.8}{2} \quad (5.8 \times 10^{-5}) = 4.3 \times 10^{-4}$$

Assuming the neutron-error distribution to be gaussian, we find

$$\delta A_{FWHM} = 12.4 \text{ amu.}$$

The resolution is

$$\frac{\delta A_{FWHM}}{\langle A \rangle} = 9.8\% \ .$$

b. Total-kinetic-energy distributions. Because neutron emission lowers the total kinetic energy in proportion to the average numbers of neutrons emitted, the pre-neutron E_K becomes:

$$E_K = E_K \text{ (observed)} \left(\frac{A_c}{A_c - \bar{\nu}} \right) .$$

The value of $\bar{\nu}$ is assumed to be

$$\bar{\nu} = \frac{E_R\ (A) + E_X - \langle E_K\ (A) \rangle}{8.3} - 1 \ ,$$

where E_R (A) is the energy released for a given mass pair, and $\langle E_K(A) \rangle$ is the mean kinetic energy for that same pair.

The alteration of the variance of the total-kinetic-energy distribution due to neutron emission may be seen as follows:

$$E_K = E_1 + E_2$$

and

$$\delta E_K = \sum_{i=1}^{\nu_1} \delta E_1 + \sum^{\nu_2} \delta E_2 ,$$

where δE is the alteration due to one neutron. We may write:

$$\mu_2 (\delta E_K) = \bar{\nu}_1 \mu_2 (\delta E_1) + \bar{\nu}_2 \mu_2 (\delta E_2) ;$$

assuming as before that the emission characteristics of the neutrons are independent of each other. Using the assumption $\nu_1 = \nu_2$, we see

$$\mu_2 (\delta E_K) = \frac{\bar{\nu}}{2} \left[\mu_2 (\delta E_1) + \mu_2 (\delta E_2) \right]$$

We need only find the variance of the error distribution for one neutron emitted by one fragment, $\mu_2 (\delta E)$. We found early in the mass-error calculations an expression for $\mu_2 (\delta E)$. Of the four terms, two were negligibly small, leaving:

$$\mu_2 (\delta E) \cong \mu_2 \left(\frac{E}{A} \right) + \frac{4}{3} m \langle E_c \rangle \left\langle \frac{E}{A} \right\rangle .$$

Treating the mass as a constant, we find

$$\left\langle \frac{E}{A} \right\rangle = \frac{\langle E_K \rangle}{A_c} \left(\frac{A_c - A}{A} \right) = \frac{\langle E_K \rangle}{A_c} \cdot R$$

and

$$\mu_2 \left(\frac{E}{A} \right) = \frac{R^2}{A_c^{\,2}} \quad \mu_2 \ (E_K) .$$

Thus we have

$$\mu_2 (\delta E) = \frac{R^2}{A_c^{\,2}} \quad \mu_2 (E_K) + \frac{4}{3} m \quad \langle E_c \rangle \ \frac{R}{A_c} \ \langle E_K \rangle .$$

Taking the example O^{16} (138 MeV) + U^{238}, we find for $R = 1$, $\mu_2 (E_K) = 3.24 \times 10^2$ and $\langle E_K \rangle = 190$ that the second term is approximately 10^2 times as large as the first. Ignoring the first term, we calculate

$$\mu_2 (\delta E) = 2.3R.$$

Then for all the neutrons and both fragments we have

$$\mu_2 (\delta E_K) = 2.3 \frac{\bar{\nu}}{2} (R + \frac{1}{R})$$

$$= 1.15 \left(\frac{E_R (A) + E_X - \langle E_K(A) \rangle}{8.3} - 1 \right) \left(\frac{R^2 + 1}{R} \right) .$$

Taking again the case O^{16} (138 MeV) + U^{238}, we find

$$\mu_2 (\delta E_K) = 39 \text{ (MeV)}^2 .$$

The loss of total-kinetic-energy resolution due to neutrons, if we assume gaussian distributions, is

$$\delta E_{K \text{ FWHM}} = 14.6 \text{ MeV},$$

which gives

$$\frac{\delta E_{K \text{ FWHM}}}{\langle E_K \rangle} = 7.7\% .$$

2. Effects of Target Thickness

The energies of fission fragments, much more than energies of lesser ionizing particles, are degraded by the fragments' passage through matter. Alexander and Gazdik have shown that for about half of their energy loss, fission fragments have ranges which follow the relationship:[33]

$$R = KE^{2/3} .$$

From the values tabulated by these authors for a given stopping material, the quantity K is found to be the same for heavy and light fragments. For small losses from the initial energy, K may be assumed to be independent of mass and dependent only on the stopping material and the energy of the fragment. Differentiating, we find

$$\frac{dE}{dR} = \frac{3}{2} \frac{E^{1/3}}{K} .$$

The mean energy loss for one fragment may then be written

$$\langle \Delta E \rangle \cong \frac{3}{2} E^{1/3} \sec \chi \sum \frac{\langle R_i \rangle}{K_i} ,$$

where χ is the angle between the target normal and the detector, and the subscript i refers to various chemical elements in the target. For each material in the target, the mean thickness is

$$\langle R_i \rangle = R_i/2 .$$

In case the fragment in question must also pass through a backing material, its average thickness is taken to be its total thickness. This mean correction was applied to the single-fragment energies during data processing (Section III.A.).

We may use the same expression to find the variance of the mass-error distribution. If an event occurs at a depth x in a target of thickness R, then one fragment will pass through target material of thickness $x \sec \chi_1$ and the other through $(R-x) \sec \chi_2$. Because:

$$\sec \chi_1 \cong \sec \chi_2 ,$$

we may approximate both by $\overline{\sec \chi}$, the average of the two. Any error in the mass may be written as

$$\frac{\delta A_1}{A_c} = \frac{E_1 \delta E_2 - E_2 \delta E_1}{E_K^{\ 2}} ,$$

where all energies are expressed in c.m. coordinates. Considering the target to be made of a single element with stopping power K, we may substitute the expression

$$\delta E \cong \frac{3}{2} \frac{E^{1/3}}{K} \delta R.$$

Here $E^{1/3}$ is expressed in lab coordinates, but because $E^{1/3}$ is a very weak function of E , we approximate

$$E^{1/3}_{lab} \cong E^{1/3}_{c.m.} .$$

Substituting the quantities

$$E_2 = \frac{A_1}{A_c} E_K$$

and

$$E_1 = \left(1 - \frac{A_1}{A_c}\right) E_K ,$$

and assuming that

$$\left(\frac{A_1}{A_c}\right)^{1/3} \cong \left(\frac{A_c - A_1}{A_c}\right)^{1/3} \cong 0.5^{1/3} ,$$

we may write

$$\frac{\delta A}{A_c} = \frac{3}{2} \frac{\overline{\sec \chi}\, 0.5^{1/3}}{K\, E_K^{2/3}} \left[\left(1 - \frac{A}{A_c}\right) x - \frac{A}{A_c} (R-x)\right].$$

This can be simplified:

$$\left[\left(1 - \frac{A}{A_c}\right) x - \frac{A}{A_c} (R-x)\right] = x - \frac{A}{A_c} R.$$

The variance of this expression is

$$\mu_2 (x) + R^2 \mu_2 (A/A_c) .$$

The distribution of x is rectangular, having a constant value from 0 to R. Thus we can write

$$\mu_2 (x) = \frac{R^2}{12} .$$

The variance of the mass-error distribution is then

$$\mu_2 \left(\frac{\delta A}{A_c}\right) = \frac{1.4\ \overline{\sec}^2\ x}{E_K^{4/3}} \left(\sum \frac{R_i}{K_i}\right)^2 \left[\frac{1}{12} + \mu_2 \left(\frac{A}{A_c}\right)\right].$$

For the case of O^{16} (138 MeV) + U^{238}, E_K = 190 MeV, we see

$$\mu_2 \left(\frac{\delta A}{A_c}\right) = 4.4 \times 10^{-6} .$$

This is negligibly small when compared with the error variance from neutron emission. If we assume the error distribution to be gaussian, we have

$$\delta A_{FWHM} = 1.2 \text{ amu} ,$$

giving a resolution

$$\frac{\delta A_{FWHM}}{\langle A \rangle} = 1.0\% .$$

Dispersion of the total-kinetic-energy distribution is seen to be negligibly small as follows. For symmetric fission, the energy lost per unit thickness traversed is equal for the two fragments. The sum of the two losses is approximately a constant regardless of the point of origin; the variance of a constant is zero. Therefore there are no first-order effects in the variance of the total-kinetic-energy distribution as there were for the mass. The only effects are second-order effects, arising from differences in energy loss by fragments of

different mass and energy. It may be concluded that these effects are very small indeed when compared with those of neutron emission.

3. Effects of Uncertainty in the Defined Laboratory Angle

It was shown in the discussion of data processing (Appendix B.2) that the c. m. and lab energies are related by

$$E_{lab} = E_{c.m.} \left(1 + x^2 + 2x \cos\theta \right) ,$$

where

$$\cos\theta = -x \sin^2\psi + \cos\psi \left(1-x^2\sin^2\psi\right)^{1/2} .$$

The calculation was based on the assumption that the lab angle ψ was well-defined. Actually, the collimation of the detector at ψ had an arc width of ±2 deg. In addition, the detector observed fragments coming from various parts of the target corresponding to an arc width of about ± 1 deg. The question we must ask is: For a number of identical fragments, each with laboratory energy E_{lab}, striking a detector with angles ranging from $\psi - \Delta\psi$ to $\psi + \Delta\psi$, what is the distribution of masses calculated from c.m. energies, which were in turn calculated on the assumption that fragments emerged at precisely ψ?

The expression for constant E_{lab},

$$E_{lab} = f\left(\cos\psi, A\right) \equiv \text{constant},$$

and

$$E_{lab} = E_c \left[1 + x^2 \left(\cos^2\psi - 1\right) + 2x\cos\psi \left(1-x^2\sin^2\psi\right)^{1/2} \right] ,$$

may be differentiated, giving

$$dE_{lab} = \left(\frac{\partial E_{lab}}{\partial A}\right)_{\cos\psi} dA + \left(\frac{\partial E_{lab}}{\partial \cos\psi}\right)_{A} d\cos\psi = 0.$$

Thus the rate of change of calculated mass with ψ is given by

$$\frac{dA}{d\cos\psi} = - \frac{\left(\frac{\partial E_{lab}}{\partial \cos\psi}\right)_{A}}{\left(\frac{\partial E_{lab}}{\partial A}\right)_{\cos\psi}} .$$

This yields a very complicated expression which must be simplified. Because the data were collected with $\psi = 90$ deg, we may use $\cos\psi = 0$ and $\sin\psi = 1$. The expression also contains the mass in a very complicated way. Because we at first want only to find the size of the effect, without being entirely general, we take only the case of symmetric fission. Then the transformation parameter becomes

$$x^2 = \frac{A_p E_p}{A_c E_K} ,$$

which for a given system is dependent only on E_K. Then we find that:

$$\frac{dA}{d\cos\psi} = - \frac{A_c x \ (1-x^2)^{1/2}}{1 + x^2} .$$

The variance of the distribution of calculated masses is then

$$\mu_2 \left(\frac{\delta A}{A_c}\right) = \left(\frac{1}{1+x^2}\right)^2 (1-x^2)\, \mu_2\, (\delta\cos\psi).$$

The distribution of $\delta\cos\psi$ appears to be complicated, because it results not only from a finite collimator, but also from a source of finite width. However, the variance of the distribution is suprisingly simple. Consider a uniform source S whose flux strikes a detector, D. The flux arising from a given point on S strikes each differential area of D with approximately equal probability. Thus the distribution of the cosines of the particles' emergent angles is approximately rectangular, with a width

$$\delta \cos\psi_{(D,S)} = \cos\,(\pi/2 - \delta\psi_{(D.S)}) - \cos\,(\pi/2 + \delta\psi_{(D,S)}).$$

The variance of the rectangular distribution is:

$$\mu_2\,(\delta\cos\psi_{(D,S)}) = \frac{(\delta\cos\psi_{(D,S)})^2}{12} .$$

Similarly a point on D observes each differential area of S with approximately equal probability. Accordingly, the cosines of all the possible angles of particles striking the point on D have a variance

$$\mu_2(\delta\cos\psi_{(S,D)}) = \frac{(\delta\cos\psi_{(S,D)})^2}{12} .$$

To a very good approximation, the point at which a particle strikes D is not related to its point of origin on S. It follows that the variance of the overall distribution of angles is the sum of the variances of the rectangular distributions. Then we can write

$$\mu_2\left(\frac{\delta A}{A_c}\right) = \left(\frac{x}{1+x^2}\right)^2 \frac{(1-x^2)}{12} \left[(\delta\cos\psi_{(D,S)})^2 + (\delta\cos\psi_{(S,D)})^2\right].$$

Using the example O^{16} (138 MeV) + U^{238}, we find

$$\mu_2\left(\frac{\delta A}{A_c}\right) = 2.0 \times 10^{-5} ,$$

which is negligible when compared with the value for neutron emission. Approximating the distribution as gaussian, we find

$$\delta A_{FWHM} = 2.7 \text{ amu} ,$$

which corresponds to a resolution of

$$\frac{\delta A_{FWHM}}{\langle A \rangle} = 2.1\% .$$

We see in the following discussion that the total kinetic energy receives only negligible dispersions from this effect. Consider two identical fission events. In the first event, fragment 1 strikes its detector at ψ_1 , and fragment 2 its detector at ψ_2 . If for the second event fragment 1 strikes its detector at $\psi_1 + \Delta\psi$, then fragment 2 strikes its detector at $\psi_2 - \Delta\psi$. The corresponding transformations to the c.m. system result in total kinetic energies $E_K = E_1 + E_2$ for the first event and $E_K' = (E_1 + \Delta E_1) + (E_2 - \Delta E_2) \cong E_K$

for the second. In the case of symmetric fission, E'_K is equal to E_K. Thus, as for finite target thickness, uncertainty of the defined angle causes no first-order terms in the energy-error distribution.

4. Detector Pulse-Height Correction

When the single-fragment energy spectra of asymmetric-fission systems are observed with semiconductor detectors, the two observed pulse-height peaks are not consistent with energies measured by time-of-flight methods or ionization chambers.[34] The pulse heights for fission fragments are lower than we would expect from a calibration line prepared from α particles. The heavy-fragment peak is farther below the calibration line than the light-fragment peak. The defect has been variously attributed to nonlinearity, an effective window on the front of the detector, or recombination of electrons and carriers in the semiconductor.

For the purposes of this work, a completely empirical correction was made. Because the peaks of the pulse-height spectra of O^{16}(165 MeV) + Au^{197} fission fragments, observed at various lab angles, gave a linear relationship when plotted against the calculated E_{lab}, it was felt no nonlinearity term was necessary. In the absence of any real knowledge about the defect, we felt it safer to err on the side of simplicity. The correction was thus based on the mass of the fragment, and was taken to be only additive. The calibration then had the form

$$E = a + b\,V + c\,(A - A_L)\ ,$$

where V is the pulse height, and A_L is the mean light-fragment mass from Cf^{252} spontaneous fission. In other words, calibration lines were a family of parallel lines, one for each mass. Without correction, the heavy-to-light mass ratio was typically 1.41. To bring this to its expected value of 1.31, a value of 0.14 MeV/amu was needed for the coefficient. This also narrowed each peak of the distribution to its expected value of 17 amu.

ACKNOWLEDGMENTS

Drs. Stanley G. Thompson and Wladislaw J. Swiatecki deserve the deepest thanks for the fruitful discussions which made this work possible.

To my wife, Phyllis, goes my heart-felt appreciation for the large volume of typing she performed, and for her continual moral support.

I wish to thank Dr. Torbjørn Sikkeland, not only for the use of his fine fission chamber, but also for the many good discussions of the experimental aspects of this work.

Contributions were made by Drs. Harry R. Bowman and J. C. D. Milton. I am especially thankful to Messers Donald S. Burnett, Reinhard Brandt, and Franz Plasil, Dr. Victor E. Viola, and Mr. J. Rayford Nix for their numerous critical discussions of all aspects of the work.

I appreciate the help of Messers Leonard E. Gibson and William W. Goldsworthy with the electronic system, especially the fast-coincidence circuity, and the help of Mr. Elwood Douglas with the two-dimensional analyzer.

This work was performed under the auspices of the U.S. Atomic Energy Commission.

REFERENCES

1. Earl K. Hyde, A Review of Nuclear Fission: Part Two - Fission Phenomena at Moderate and High Energy, UCRL-9065, February 1960, pp. 7a, 27, 57, and 59.
2. E. Segre and C. Wiegand, Phys. Rev. 94, 157 (1954).
3. John S. Wahl, Phys. Rev. 95, 126 (1954).
4. Edward L. Hubbard, Ann. Rev. Nucl. Sci. 11, 419 (1961).
5. Edward L. Hubbard et al., Rev. Sci. Instr. 32, 621 (1961).
6. L. C. Northcliffe, Phys. Rev. 120, 1744 (1960).
7. J. L. Blankenship, "Surface Barrier Detectors," in Semiconductor Nuclear Particle Detectors, Proceedings of an Informal Conference, edited by J. S. T. Dabbs and F. J. Walter, Asheville, N. C., Sept. 28-30, 1960, (National Academy of Sciences-National Research Council, Washington, D. C., Publication 871, 1961).
8. H. R. Bowman, S. G. Thompson, J. C. D. Milton, and W. J. Swiatecki, Phys. Rev. 126, 2120 (1962).
9. H. R. Bowman, J. C. D. Milton, S. G. Thompson, W. J. Swiatecki, Further Studies of the Prompt Neutrons from the Spontaneous Fission of Cf^{252}, UCRL-10139, May 1962 submitted to Phys. Rev.
10. Eldon L. Haines, "Mass-Yield Curve for Fission in the Reaction C^{12} (112 MeV) + U^{238} → Fission," in Chemistry Division Annual Report, UCRL-9566, p. 106.
11. R. D. Present, Phys. Rev. 72, 7 (1947).
12. H. C. Britt, H. E. Wegner, and J. Gursky, Energetics of Charged-Particle-Induced Fission Reactions (Los Alamos Scientific Laboratory, unpublished work).
13. Reinhard Brandt, Lawrence Radiation Laboratory, private communication.
14. J. C. D. Milton and J. S. Fraser, Phys. Rev. 111, 877 (1958).
15. V. E. Viola and T. Sikkeland, Lawrence Radiation Laboratory, private communication.
16. Walter M. Gibson, Bell Telephone Laboratory, private communication.

17. T. Sikkeland, E. L. Haines, and V. E. Viola, Phys. Rev. 125, 1350 (1962).

18. John R. Hiskes, The Liquid-Drop Model of Fission: Equilibrium Configurations and Energetics of Uniform Rotating Charged Drops (Thesis), UCRL-9275, June 1960.

19. G. A. Pik-Pichak, Soviet Phys. J. E. T. P. 38, 768 (1960).

20. R. Vandenbosch and J. R. Huizenga, "Competition Between Fission and Neutron Emission as a Function of Excitation Energy and Nuclear Type," Paper P/688, in Proceedings of the Second International Conference on the Peaceful Uses of Atomic Energy, Geneva 1958 (United Nations, New York, 1958), Vol. 15, p. 284.

21. T. Sikkeland, S. Amiel, and S. G. Thompson, Spallation Reactions of Californium-252 with Helium Ions, UCRL-8103 Rev., February 1959.

22. G. N. Flerov, Recent Research on Fission Performed at the Institute of Atomic Energy of the USSR Academy of Sciences, Moscow, in Proceedings of the Conference on Reactions between Complex Nuclei, edited by A. Zucker, R. S. Livingston, and F. T. Howard, ORNL-2606, Oct. 1958, p. 384.

23. William W. Goldsworthy, Model VI Linear Amplifier System and Preamplifier, UCRL-9816, August 1961.

24. Lawrence Radiation Laboratory Counting Handbook, UCRL-3307 Rev., January 1959, File No. CC1-4.

25. Ref. 24, File No. CC3-10.

26. Ref. 24, File No. CC3-11.

27. R. B. Leachman, in Proceedings of the Second International Conference of the Peaceful Uses of Atomic Energy, Geneva, 1958 (United Nations, New York, 1958), Vol. 15, p. 229.

28. A. Hald, Statistical Theory with Engineering Applications (John Wiley and Sons, Inc., New York, 1952).

29. J. C. Douglas Milton, Chalk River Project, Atomic Energy of Canada Limited, Chalk River, Ontario, Canada, private communication.

30. See also Appendix III from James Terrell, Neutron Yields from Individual Fission Fragments, (to be submitted to the Physical Review).

31. J. C. Douglas Milton, Fission Energy Tables and an Application to Nuclear Charge Division, UCRL-9883 Rev., January 1962.

32. G. R. Choppin, B. G. Harvey, D. A. Hicks, J. Ise, and R. V. Pyle, Phys. Rev. 102, 766 (1956).

33. J. M. Alexander and M. F. Gazdik, Phys. Rev. 120, 874 (1960).

34. See for example Semiconductor Nuclear Particle Detectors, Proceedings of an Informal Conference, Asheville, N. C., Sept. 28-30, 1960, J. S. T. Dabbs and F. J. Walter, Eds. (National Academy of Sciences--National Research Council, Washington, D. C., 1961), Pub. 871, p. 6.

This report was prepared as an account of Government sponsored work. Neither the United States, nor the Commission, nor any person acting on behalf of the Commission:

A. Makes any warranty or representation, expressed or implied, with respect to the accuracy, completeness, or usefulness of the information contained in this report, or that the use of any information, apparatus, method, or process disclosed in this report may not infringe privately owned rights; or

B. Assumes any liabilities with respect to the use of, or for damages resulting from the use of any information, apparatus, method, or process disclosed in this report.

As used in the above, "person acting on behalf of the Commission" includes any employee or contractor of the Commission, or employee of such contractor, to the extent that such employee or contractor of the Commission, or employee of such contractor prepares, disseminates, or provides access to, any information pursuant to his employment or contract with the Commission, or his employment with such contractor.